



Call: H2020-SC5-2014-two-stage

Topic: SC5-01-2014

**PRIMAVERA**

Grant Agreement 641727



**PRocess-based climate sIMulation: AdVances in high resolution modelling and  
European climate Risk Assessment**

**Deliverable D5.3 - Appendix**

***Impact of sea ice and snow changes on European climate  
of the most recent period and its sensitivity to resolution  
and physics choices***

## Appendix A: Results from forced Arctic sea ice decline in coupled experiments

### Report from CERFACS, UCLouvain, ECMWF

The atmospheric response to Arctic sea ice decline is analysed with two coupled models at low and high resolutions : ECMWF-IFS-LR, ECMWF-IFS-HR, CNRM-CM6.1-LR and CNRM-CM6.1-HR. In all the experiments, the albedo of sea ice is reduced to the ocean value in a 40 member-ensemble (PERT) initialised from the control-1950 experiment (CTRL). The spatial distribution and the seasonal cycle of sea ice loss (PERT - CTRL) are represented in Fig. A.1 and in Fig. A.2 for the 4 experiments. The amount of sea ice loss is stronger in LR models than in HR, because HR models have a warmer mean state over the Arctic Ocean with less sea ice in their control experiment (Fig. A.1). However, when comparing to the control experiment, sea ice loss is equivalent in LR and HR. Reducing sea ice albedo leads to a 100% reduction in summer in the CNRM-CM6.1 model and only 30% in ECMWF-IFS.

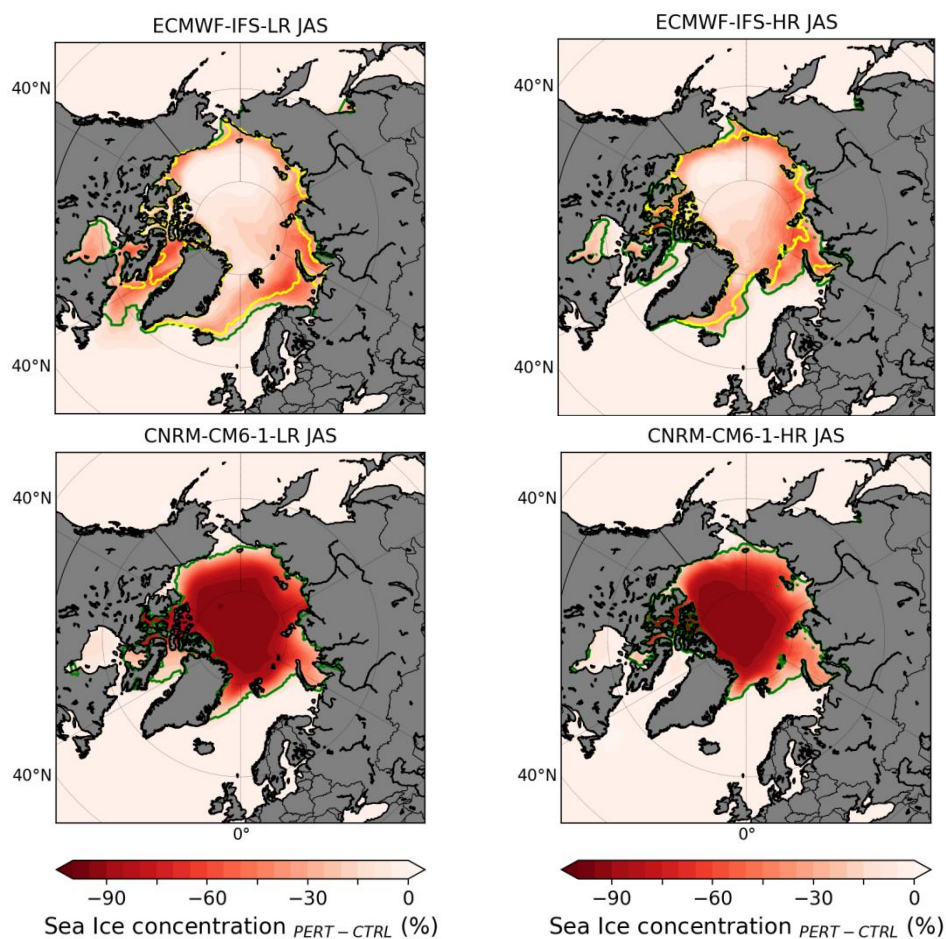


Figure A.1: Spatial distributions of sea ice concentration loss (PERT-CTRL) averaged over the 40 member-ensemble in summer (JAS) in ECMWF-IFS-LR, ECMWF-IFS-HR, CNRM-CM6.1-LR and CNRM-CM6.1-HR. The green line and the yellow line show the sea ice edge (15% concentration) for the CTRL and the PERT respectively.

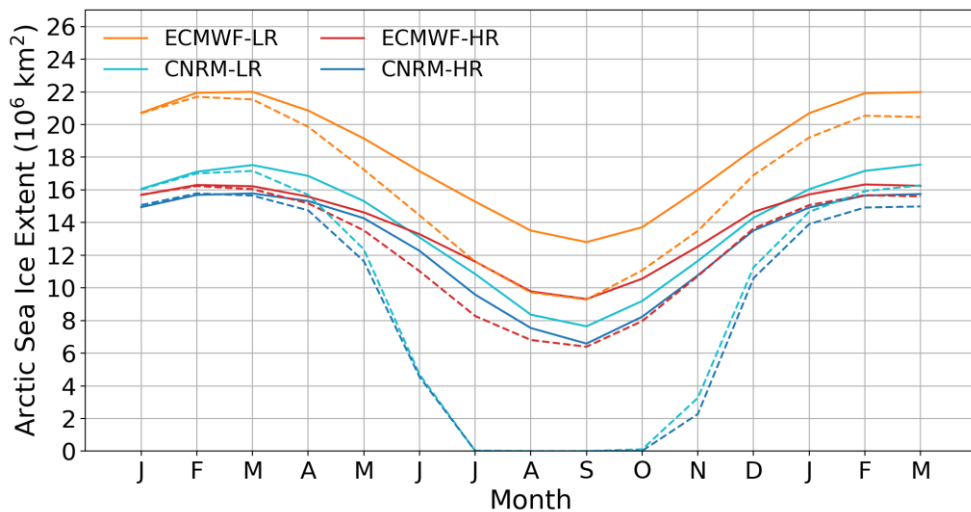


Figure A.2: Seasonal cycles of the mean Arctic sea ice extent for the CTRL in solid lines and for the PERT in dotted lines.

In response to Arctic sea ice decline a strong warming is found over the Arctic Ocean in the 4 experiments in JFM (Fig. A.3) and it extends to the adjacent continents as far as Canada, Scandinavia and northern Russia. Generally, the near-surface atmospheric responses are very similar between the two resolutions of the CNRM-CM6.1 and ECMWF models respectively, indicating that the effect of horizontal resolution is small in this response for the models analyzed here. Note that different experiments done within the PAMIP project suggest that increasing the horizontal resolution to scales finer than 25 km in the atmosphere can yield a different response to sea ice loss. A robust cooling is found over Eastern Eurasia in both models and for both resolutions (Fig. A.3). This cooling is however more spatially restricted in the higher resolution version of CNRM-CM6.1 than at lower resolution and less intense in ECMWF-IFS. Over high latitudes, all the models seem to be in agreement except that the warming extends further south in LR models. In regions south of 70°N, the warming is more important in LR for the two models (Fig. A.4). That can be easily explained by more sea ice loss in the LR models as seen in Fig. A.1 and especially over the marginal sea ice zone.

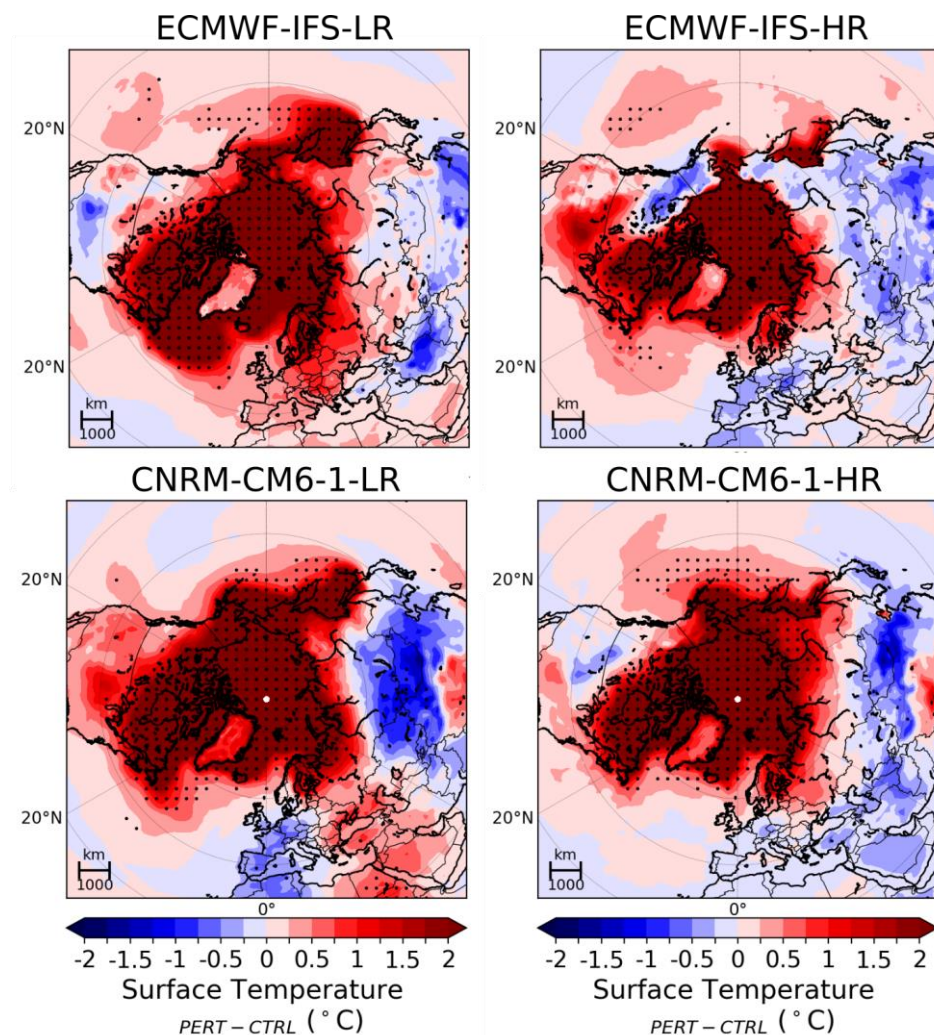


Figure A.3: Near-surface atmospheric response in winter (JFM) in ECMWF-IFS-LR, ECMWF-IFS-HR, CNRM-CM6.1-LR and CNRM-CM6.1-HR. Dots: Statistically significant points at the 5% level using the Kolmogorov-Smirnov test and accounting for the False Discovery Rate (FDR) (Wilks 2016)

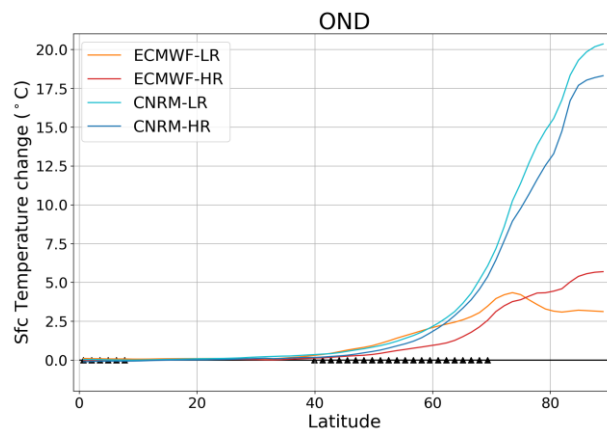


Figure A.4: Latitudinal cross-section of the zonal mean surface temperature response for all configurations in autumn. If the difference between the two models (two resolutions combined) is statistically significant for the Kolmogorov-Smirnov test at the 5% level at a given latitude, a black triangle is represented.

Figure A.5 shows the precipitation response in autumn. An increase over the Arctic marginal sea ice zone is observed in all configurations because new open water areas occur in PERT over these regions. It leads to an increase in evaporation, resulting in enhanced precipitation in these new open water areas, confirming previous studies. Moreover, even if the mean response over the western coast of the US differs between the configurations, an increase in drought duration is detected in all configurations except CNRM-CM6.1-HR in December (not shown). The precipitation responses, except in some regions over the Arctic, are not statistically significant suggesting both a small signal and a large internal variability for this variable.

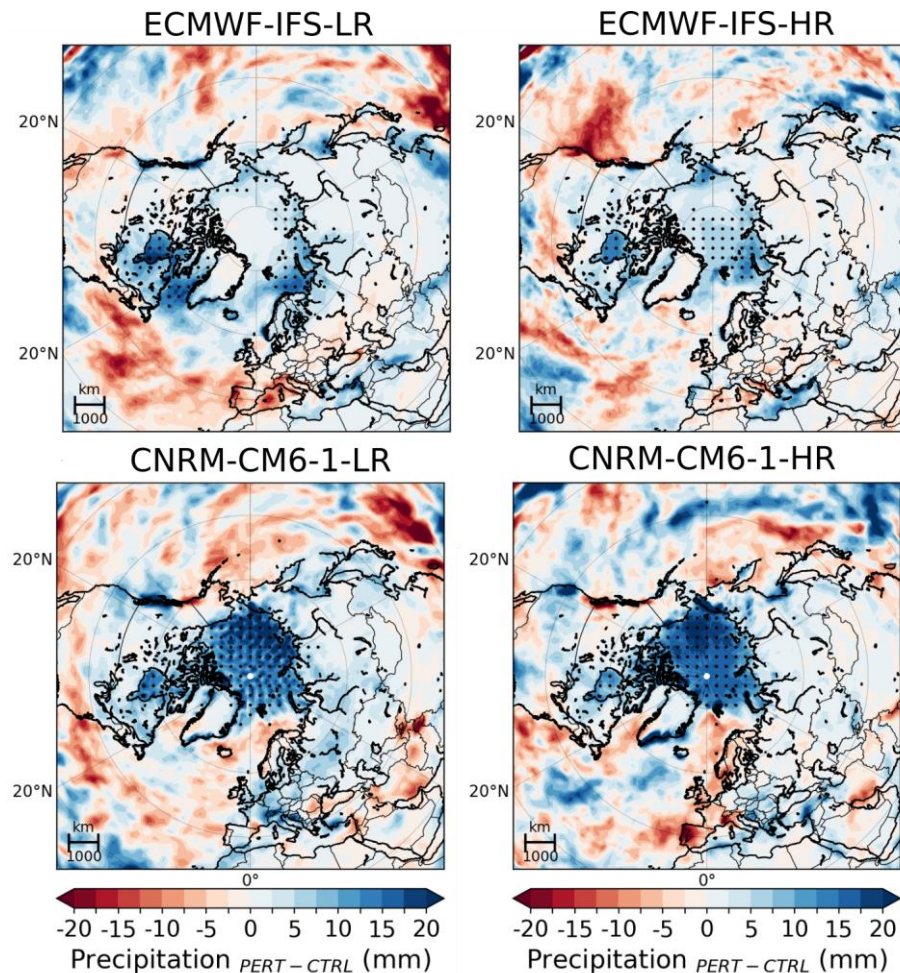


Figure A.5: Same as Fig. A.3 but for the precipitation response in OND

Regarding the sea level pressure response (Fig. A.6), a strong cyclonic anomaly occurs over the Arctic Ocean in autumn (OND) when Arctic amplification is the strongest. This anomaly is stronger in LR than in HR, in line with the intensity found for sea ice loss and Arctic amplification. Elsewhere, the response is different among the 4 cases but the response is very weak and hardly significant.

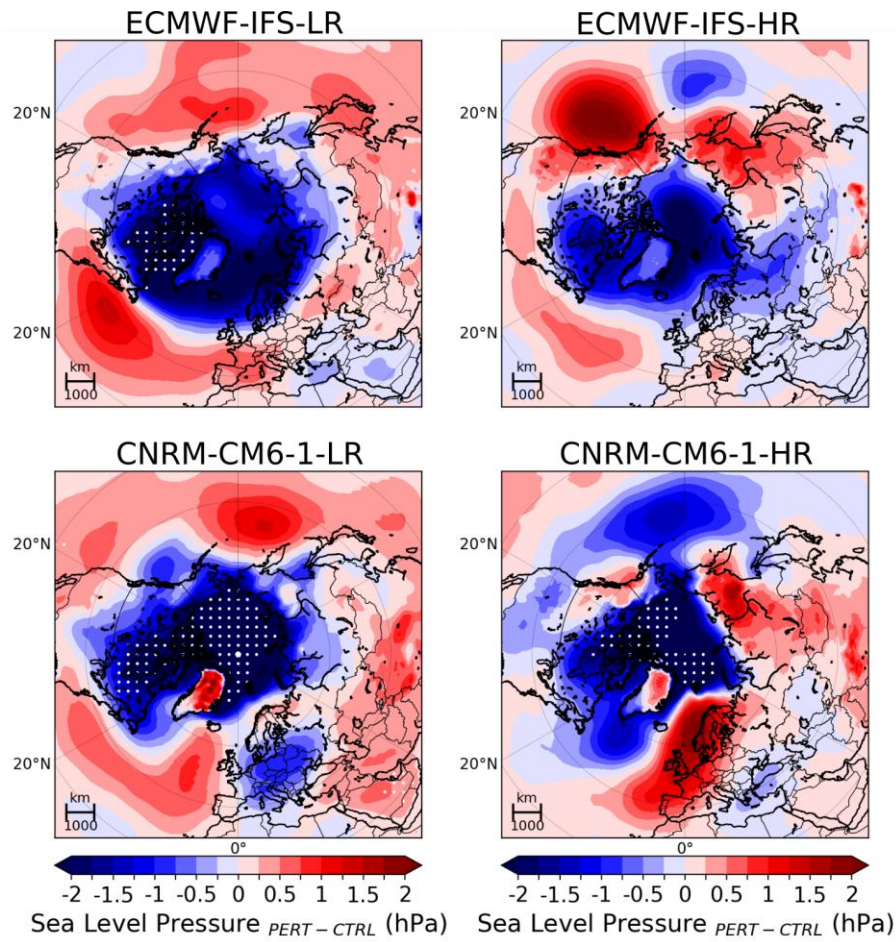


Figure A.6: Same as Fig. A.5 but for the sea level pressure

A weakening of the stratospheric polar vortex is seen with a reduction of the zonal-mean zonal winds in response to Arctic sea ice loss (Fig. A.7). This weakening occurs at different months between the ECMWF-IFS and CNRM-CM6.1 models. In ECMWF-IFS, it occurs in late winter whereas in CNRM-CM6.1 it occurs in December in the lower part of the polar vortex. In both models, the responses are consistent for both resolutions, but the weakening is stronger in HR. Moreover, in ECMWF-IFS the decrease in zonal winds occurs up to the low troposphere in HR only, which is consistent with more extensive cooling patterns into mid-latitudes compared to LR (Fig. A.3). However, the zonal-mean zonal wind responses are not statistically significant in any of the 4 experiments.

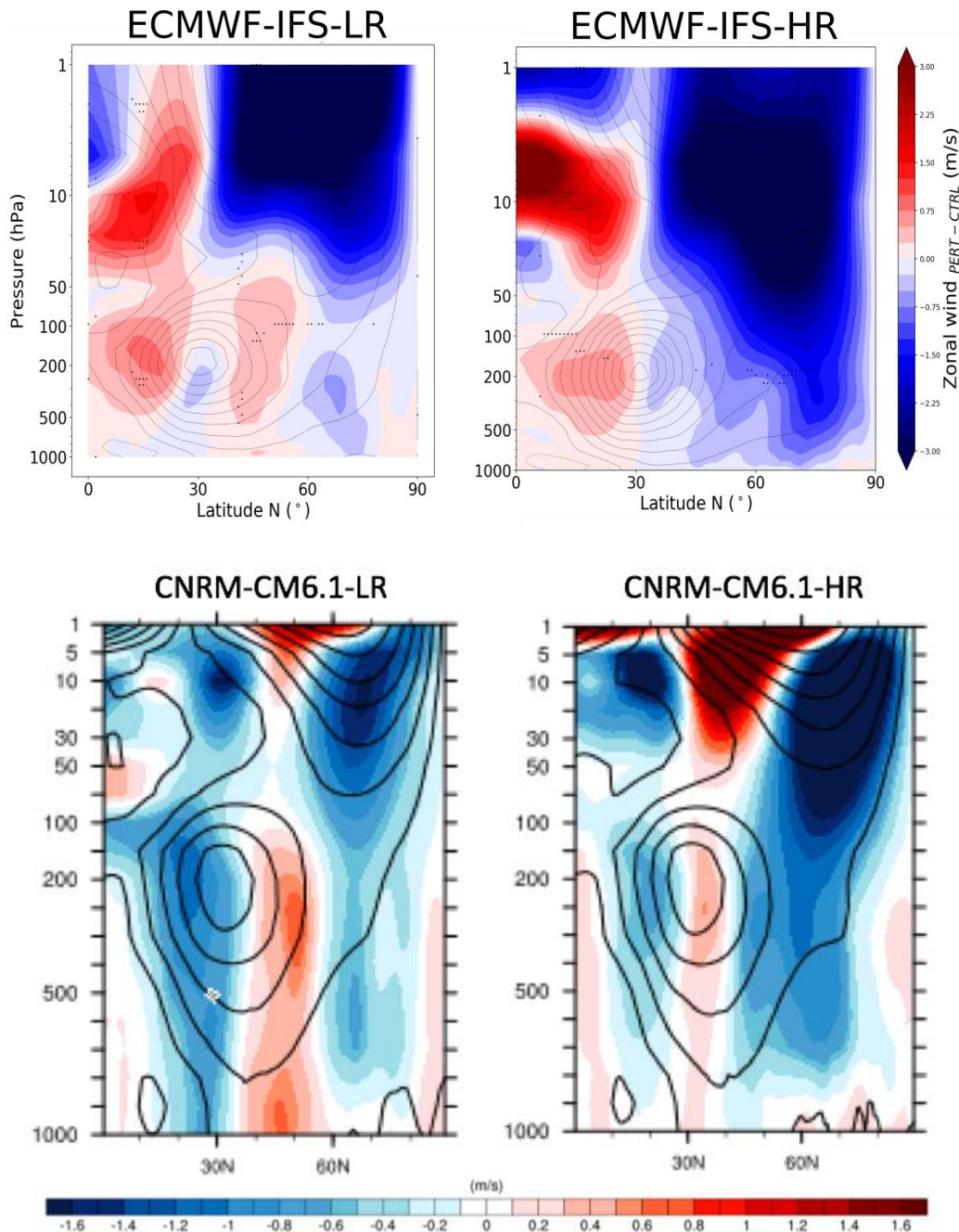


Figure A.7: Zonal-mean zonal winds in March in ECMWF-IFS-LR, in February in ECMWF-IFS-HR, in December in CNRM-CM6.1-LR and CNRM-CM6.1-HR (the response is not significant using a two-sided Student t-test and the FDR). Dots in ECMWF : statistically significant points at the 5% level using the Kolmogorov-Smirnov test only.

The different patterns and timings of the response between both resolutions and both models are probably due to different mean states and different amounts of sea ice loss. First, the amount of sea ice loss and particularly the location of this loss can produce different atmospheric impacts in ECMWF-IFS such as the stratospheric weakening as previously shown. Moreover, in ECMWF-IFS-LR a loss of sea ice is observed south of the Labrador Sea in winter, which produces a decrease in sea level pressure over this region in

this model particularly. This explains the discrepancy found for the North Atlantic circulation when comparing ECMWF-IFS-LR with other configurations. Note also that the maximum of sea ice loss occurs at different months between CNRM-CM6.1 (October/November) and ECMWF-IFS (July/August), which could partly explain the different timings of the stratospheric zonal-mean zonal wind response between the 2 models (Fig. A.7, December in CNRM-CM6.1 for both resolutions, February in ECMWF-IFS-HR and March in ECMWF-IFS-LR). The different atmospheric mean states could also explain the different timing of the response. Further, the more marked weakening of the zonal-mean zonal winds in the stratosphere at a higher resolution in CNRM-CM6.1 could be linked to a reduced variance of the polar vortex (Fig. A.8).

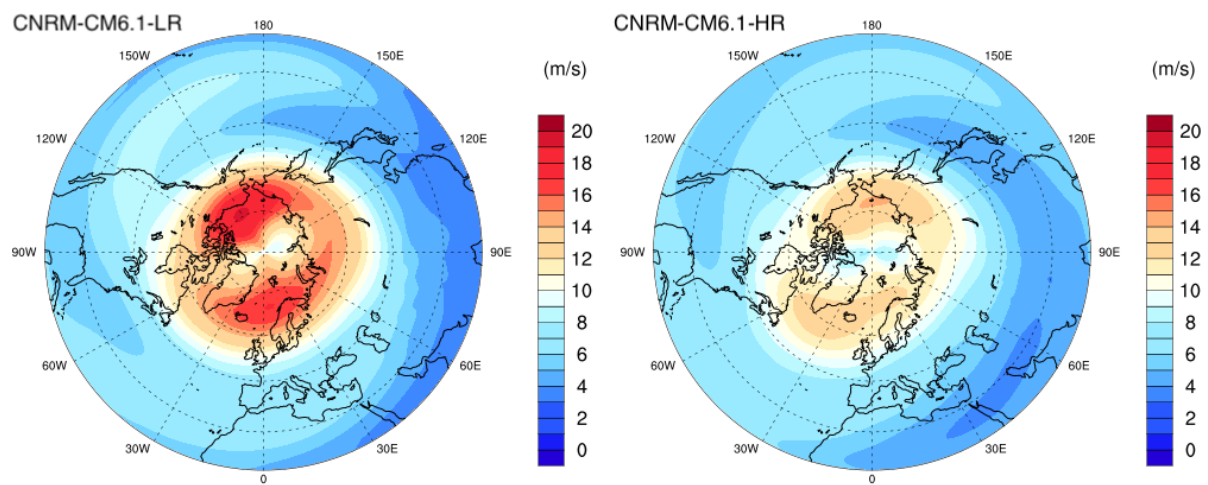


Figure A.8: Standard deviation of the stratospheric polar vortex (zonal-mean zonal wind at 10 hPa) in CTRL in CNRM-CM6.1-LR (left) and CNRM-CM6.1-HR (right).

The uncertainty in the ensemble mean is usually lower for high resolution models for a given number of members compared to low resolution models for the surface temperature and the sea level pressure response over Europe (Fig. A.9). It suggests that less members are needed to detect a significant sea level pressure and temperature responses due to sea ice loss in high resolution models. Indeed, the ensemble size is lower in these models to reach a statistically significant mean response (Fig. A.9). This is consistent with the evolution of the near-surface temperature response in the CNRM-CM6.1 model at both resolutions and for different combinations of members (Fig. A.10): the Eastern Eurasia cooling is significant with 200 members in LR and with 120 members in HR, indicating a more rapid convergence of this response with the high resolution model. Note that this cooling is more spatially restricted when the number of members is larger than 40 but also when increasing the resolution and keeping only 40 members. In the stratosphere, the weakening of the lower part of the polar vortex in this model is also stronger in HR than in LR for different combinations of members, and significant in the uppermost levels from 120 members. Hence, less members are needed in HR to have a more robust stratospheric response.

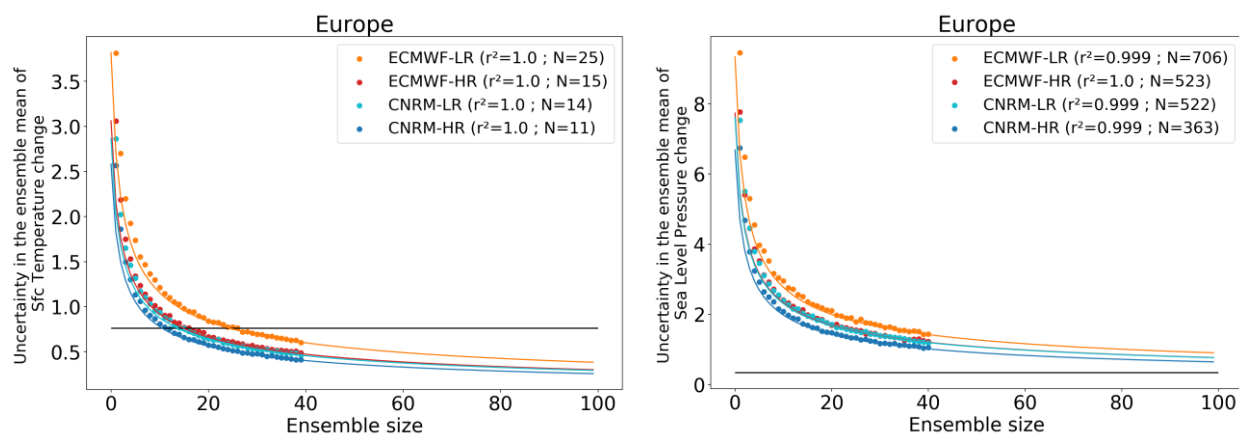
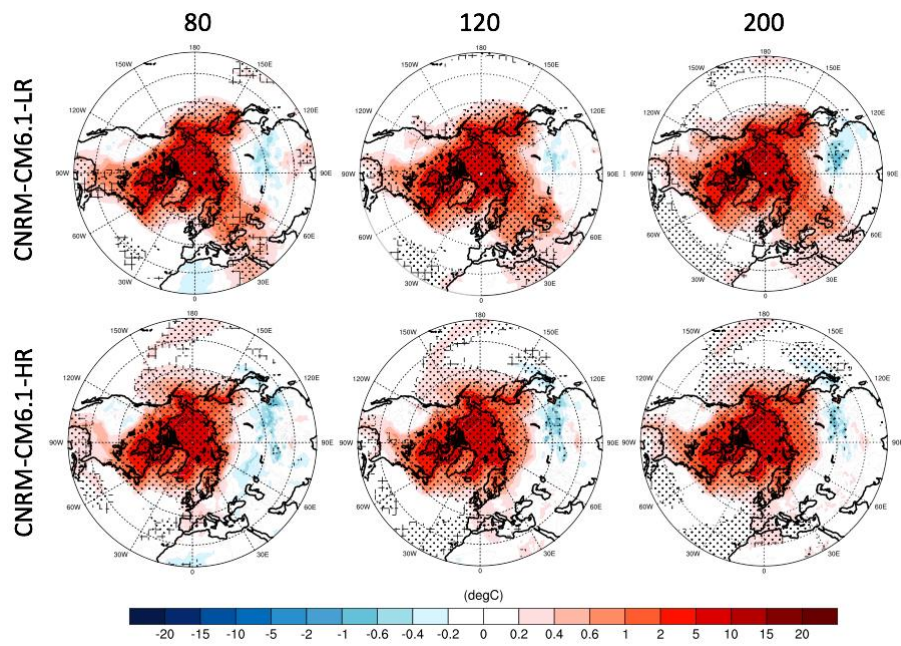


Figure A.9: Uncertainty in the ensemble mean as a function of the ensemble size on the mean response of the surface temperature (left), and of the sea level pressure (right) for all the models over Europe. The dots represents the uncertainty for the real sample of data, and the curves represents a power law model ( $Y=aX^b$ ), which fit the dots as best as possible. The black line represents the mean response for all the configurations and N illustrates the ensemble size required to reach the mean response.

(a)



(b)

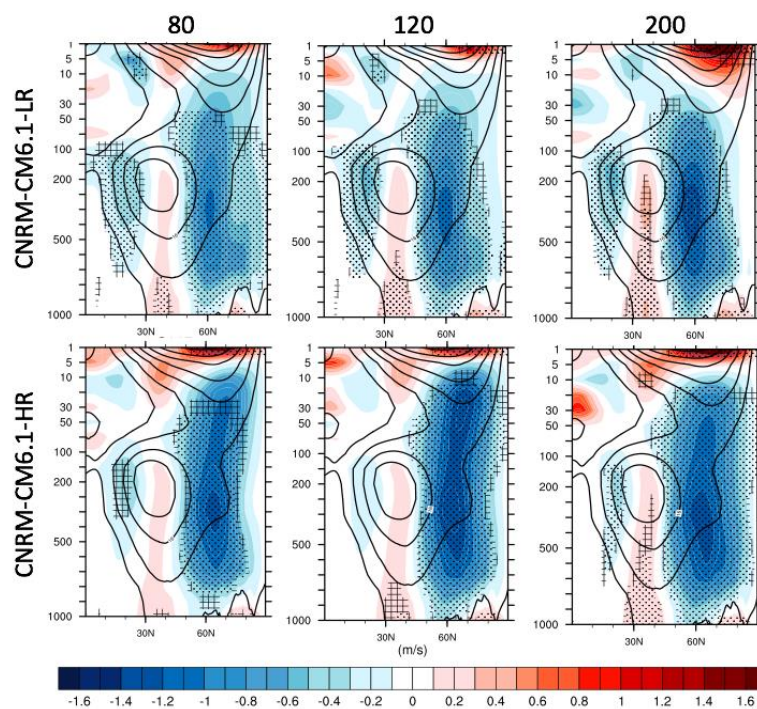


Figure A.10: Near-surface atmospheric response in JFM (a) and zonal-mean zonal wind response in OND (b) in CNRM-CM6.1-LR and CNRM-CM6.1-HR for different combinations of members (80, 120, 200). Interval for contours in (b): 8 m/s.

Internal variability is clearly dominant in these experiments with 40 members compared to model or resolution uncertainty even for surface temperature responses, except over the Arctic. Over Europe, the internal variability uncertainty determined by the standard deviation on the 40 members represents around 80% of the total uncertainty regardless of the variable used (Fig A.11).

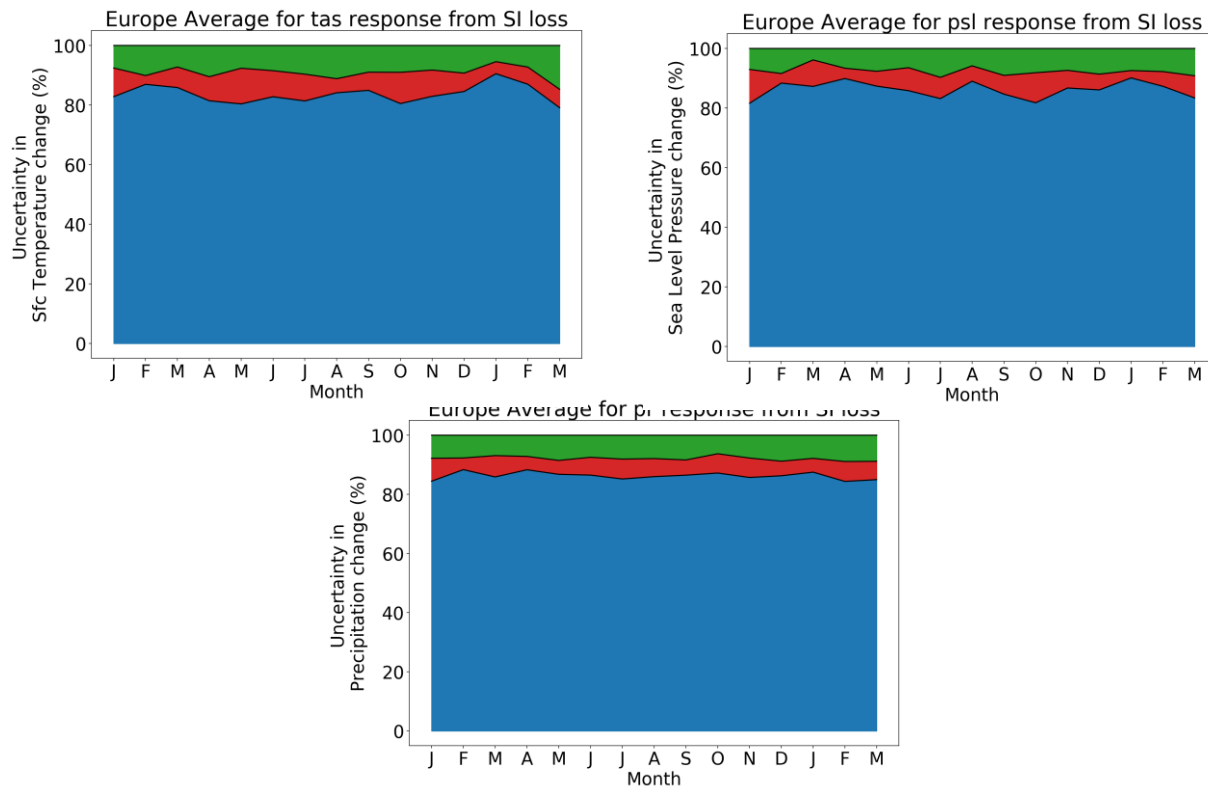


Figure A.11 : The relative uncertainty (on the spread) of each source averaged over Europe for the surface temperature, the precipitation and the sea level pressure response. Blue represents the uncertainty due to internal variability, red represents the model uncertainty and green represents the resolution uncertainty.

In summary, the atmospheric responses to Arctic sea ice decline in the ECMWF-IFS and CNRM-CM6.1 models are similar over statistically significant areas in low and high resolutions, and between the 2 models. Increasing horizontal resolution has a relatively weak impact on the pattern of the atmospheric response but it seems to favor more rapidly the convergence of a robust response. However, considering these experiments with only 40 members does not enable to separate the precipitation and the sea level pressure responses out of the Arctic due to sea ice loss from the internal variability of the climate. Indeed, the stratospheric response is not significant and the sea-level pressure and precipitation responses are very weak and hardly significant. We have extended the number of members to 200 with the CNRM-CM6.1 model and showed that we need at least 120 members to get a significant response in the stratosphere and to get significant and similar sea level pressure responses in both resolutions.

## Appendix B: Results from prescribed sea-ice changes in atmosphere-only experiments

### Report from CERFACS

The set of AMIP-type experiments performed with the atmospheric component of the CNRM-CM6-1 model under WP5 will focus on the impact of Arctic sea-ice on the European climate. We have performed a set of 10 AMIP (*PERT*) atmospheric experiments at both low- and high resolution (hereafter LR and HR). These experiments are a shorter variation of the AMIP experiments (the control ones, *CTRL*) performed under WP6. They only cover the 1991-2014 period, corresponding to a trend towards reduced Arctic sea-ice. Instead of having the Arctic sea ice extent varying with time, we will prescribe each year the observed climatology from 1979-1990. Comparison with the control experiments leads to an assessment of the potential influence of Arctic sea-ice on the European climate for the recent period.

Here we focus on the period 1995-2014 during which Arctic sea-ice loss has been the most pronounced (changing the period by going back to 1991 or reducing it to 2000-2014 has no significant influence on the results). In the following we show the ensemble mean (over the period 1995-2014) difference *CTRL – PERT* which can be simply interpreted as the mean influence of Arctic sea-ice loss on the European climate. Note that the difference is therefore estimated from a total number of 200 years for each ensemble. We systematically show differences at both resolutions and assess statistical significance at the 5% level (as in Terray et al. 2004).

**Figure B.1** shows the simulated (at low-resolution) influence of Arctic sea-ice loss on 2-meter air temperature (T2m) for the 4 seasons (JFM, AMJ, JAS and OND). Sea-ice loss warms the Arctic lower troposphere in all seasons with the largest amplitude in Autumn (~2-3°C) over the Barents-Kara (BKS) and Chukchi seas as well as Baffin Bay and the Canadian Archipelago. The largest (and significant) land warming over northern and central Eurasia is mostly in Autumn and Winter. Mid-latitude Eurasia displays a low-amplitude (~ 0.4°C) cooling (weakly significant only in Autumn). Based on our LR model, Arctic sea-ice loss has almost no influence on Western Europe but in Summer with a low-amplitude warming. The same analysis with the HR-version leads to almost similar results (**Figure B.2**). Autumn still shows the largest temperature positive anomalies over the Arctic (Winter and Summer display slightly reduced warming in the central Arctic compared to the LR-version). The cooling over Eurasia in Autumn is not significant in the HR-version. **Figure B.3** shows that the difference based on the HR-version for precipitation is rather weak, without clear large-scale spatial patterns and not significant.

A key example of mid-latitude regional climate change across the historical period is the winter Central and Eastern Eurasia land cooling of the late-20th century until around 2014. This recent cooling episode disrupted the warming trend that started in the early 1970s and is in striking contrast to the concurrent Arctic amplification (the

propensity for greater surface warming in the Arctic region than at other latitudes) and sea-ice decline. Here we focus on the hiatus period defined as 1998–2014 during which the mid-to-high latitudes of the Eurasian continent cooled significantly in winter. We use the *CTRL* and *PERT* experiments (using both LR and HR model versions) to assess the potential influence of Arctic sea-ice decline on the Eurasian cooling.

Some studies have suggested that Arctic sea-ice decline could have significantly contributed to the Eurasian cooling (e.g Mori et al. 2014) while others have claimed that internal (and in particular atmospheric) variability is the main contributor (e.g Sun et al. 2016). **Figure B.4** shows winter (JFM) temperature trends for the low-resolution version of *CTRL* and *PERT* as well as the observations/reanalyses (here ERA-Interim). The observations show a clear dipolar pattern with a warming trend along the Arctic coast of Eurasia and a strong midlatitude cooling extending from Europe to East Asia. This cooling is due to a strengthening and shift of the Siberian High that favours advection of cold Arctic air masses and blocks the inflow of the mild and wet Atlantic westerly flow. The sea level pressure (SLP) trend pattern is reminiscent of the negative phase of the North Atlantic Oscillation. An anticyclonic anomaly is also depicted in the North Pacific and contributes to the cooling of Alaska, Canada and the northern United States. Both ensemble mean trends (*CTRL* and *PERT*) reproduce in a similar way the North Pacific SLP blocking anomaly (and the associated North America cooling) suggesting that it is primarily due to sea surface temperature (SST) forcing (it can be shown that this is mainly due to the change in Pacific Decadal Oscillation phase during the period).

In contrast, none of the ensemble mean trends is able to reproduce the strong blocking high (intensification of the Siberian High) and the related intense midlatitude Eurasian cooling seen in the observations. Furthermore, *CTRL* (with Arctic sea-ice loss) exhibits a clear warming trend over Eurasian midlatitudes while *PERT* (with no Arctic sea-ice loss) shows a mix of very weak positive and negative trends. Along the Arctic coast, *CTRL* shows a much stronger land warming than *PERT* suggesting that sea-ice loss did indeed play a role in the observed warming. Quasi-similar results are obtained with the HR-version (**Figure B.5**).

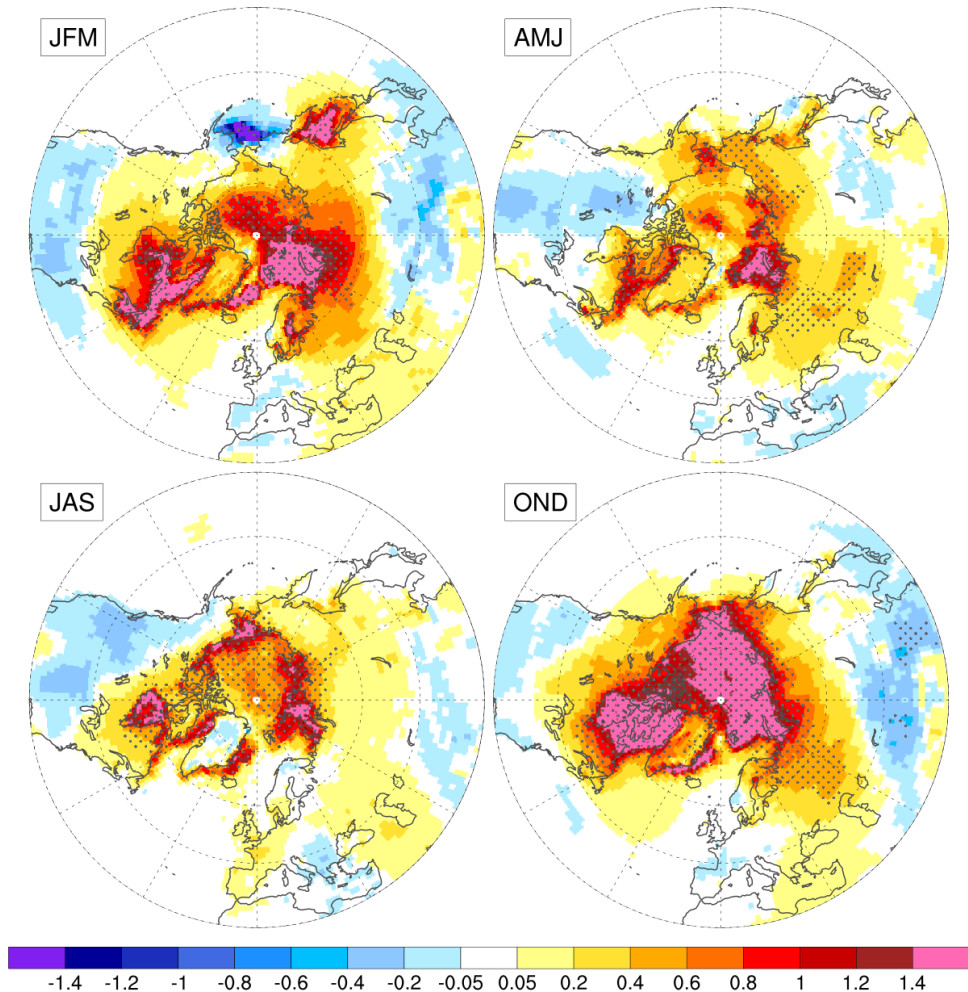
In summary, the results based on both LR and HR versions suggest that recent Arctic sea-ice loss has largely contributed to the observed lower tropospheric Arctic warming. In contrast, they also suggest that sea-ice loss cannot be a significant (much less the main) factor of the observed Eurasian winter cooling during 1998–2014. Therefore, they suggest that internal variability is likely to be the dominant factor of the Eurasian cooling. These results agree to a large extent with recent multi-model atmospheric results obtained in the GREENICE project (albeit with a slightly different protocol and other models), for instance Ogawa et al. 2018 and see also Sun et al. 2016 and Blackport et al. 2019.

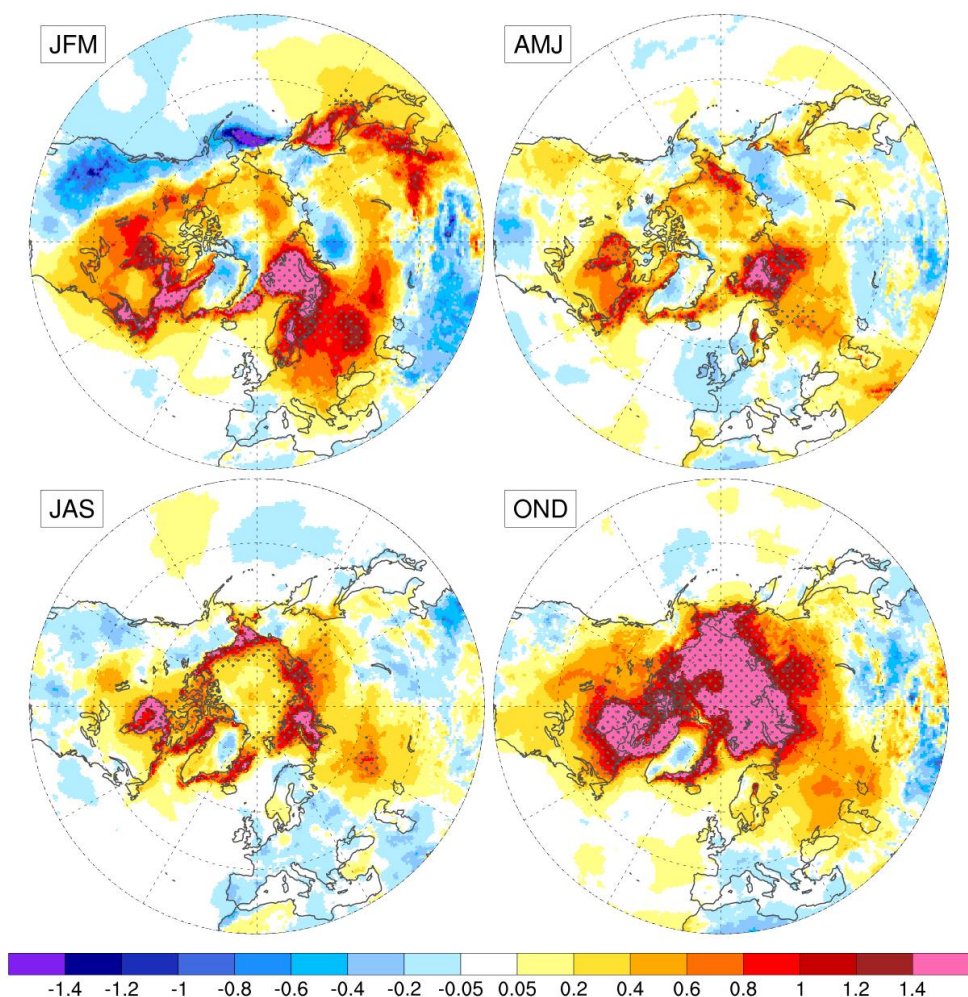
**References:**

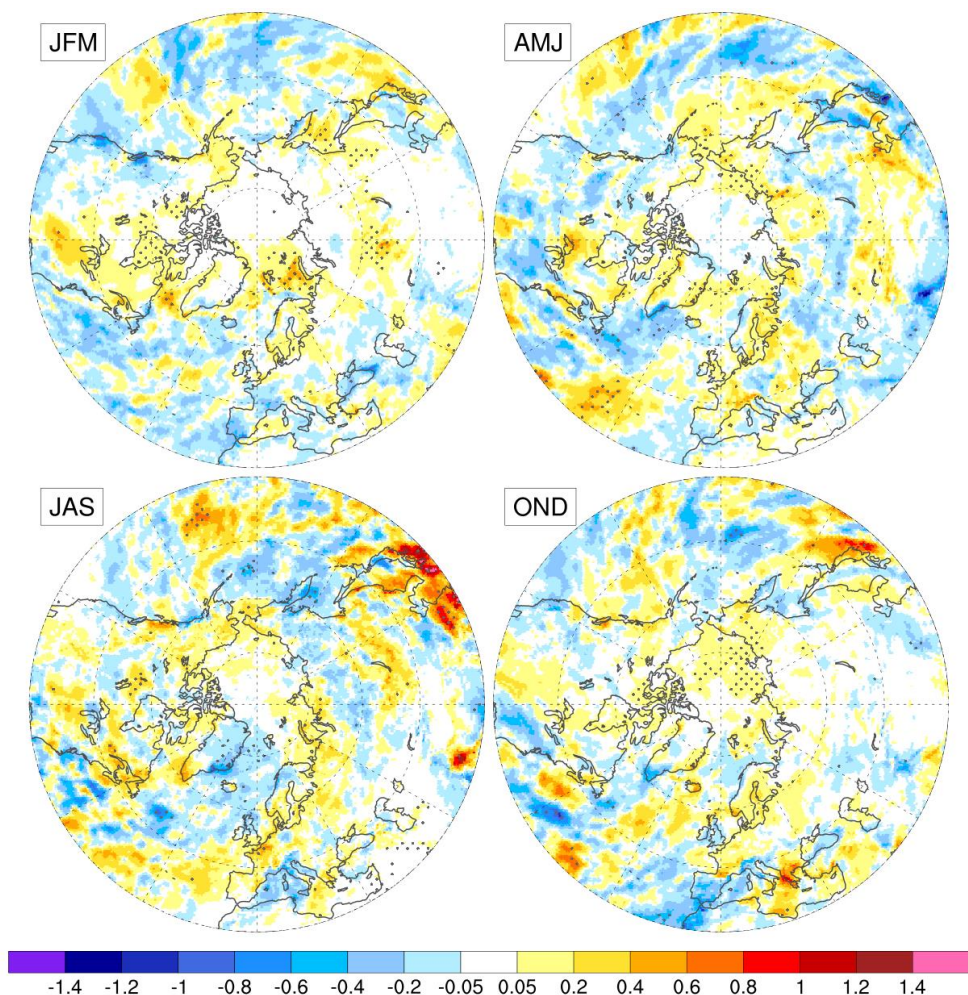
- Blackport, R., Screen, J. A., van der Wiel, K., and Bintanja, R. (2019). Minimal influence of reduced Arctic sea ice on coincident cold winters in mid-latitudes. *Nat. Clim. Chang.* 9, 697–704. doi:10.1038/s41558-019-0551-4.
- Mori, M., Watanabe, M., Shiogama, H., Inoue, J., and Kimoto, M. (2014). Robust Arctic sea-ice influence on the frequent Eurasian cold winters in past decades. *Nat. Geosci.* 7, 869–873. doi:10.1038/ngeo2277
- Ogawa, F., Keenlyside, N., Gao, Y., Koenigk, T., Yang, S., Suo, L., et al. (2018). Evaluating impacts of recent Arctic sea ice loss on the northern hemisphere winter climate change. *Geophysical Research Letters*, 45, 3255–3263. <https://doi.org/10.1002/2017GL076502>
- Sun, L., Perlitz, J., and Hoerling, M. (2016). What caused the recent “Warm Arctic, Cold Continents” trend pattern in winter temperatures? *Geophys. Res. Lett.* 43, 5345–5352. doi:10.1002/2016GL069024.
- Terray, P., Delecluse P., Labattu S., and Terray L., (2003) *Sea Surface Temperature associations with the Late Indian Summer Monsoon Climate Dynamics*, vol. 21, 593-618 pp., doi: [10.1007/s00382-003-0354-0](https://doi.org/10.1007/s00382-003-0354-0)

## Figures

**Figure B.1:** 20-year (1995-2014) mean surface air temperature ( $^{\circ}\text{C}$ ) difference  $\text{CTRL} - \text{PERT}$  based on the low-resolution experiments. Stippling indicates significant differences at the 5% level.



**Figure B.2:** as in **Figure B.1** but for the high-resolution experiments

**Figure B.3:** same as **Figure B.2** but for precipitation ( $\text{mm day}^{-1}$ )

**Figure B.4:** Winter (JFM) temperature and sea level pressure linear trends (units  $^{\circ}\text{C} 17\text{yrs}^{-1}$  & hPa  $17\text{yrs}^{-1}$ ) over the 1998-2014 period. From left to right: *CTRL* ensemble mean trend, *PERT* ensemble mean trend and ERA-Interim. *CTRL* and *PERT* are from the low-resolution version of CNRM-CM6-1.

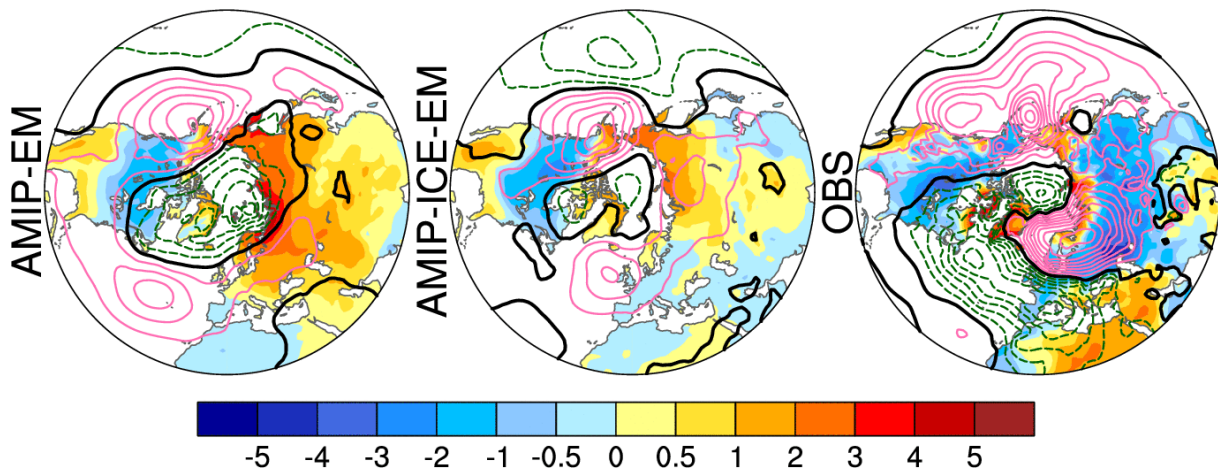
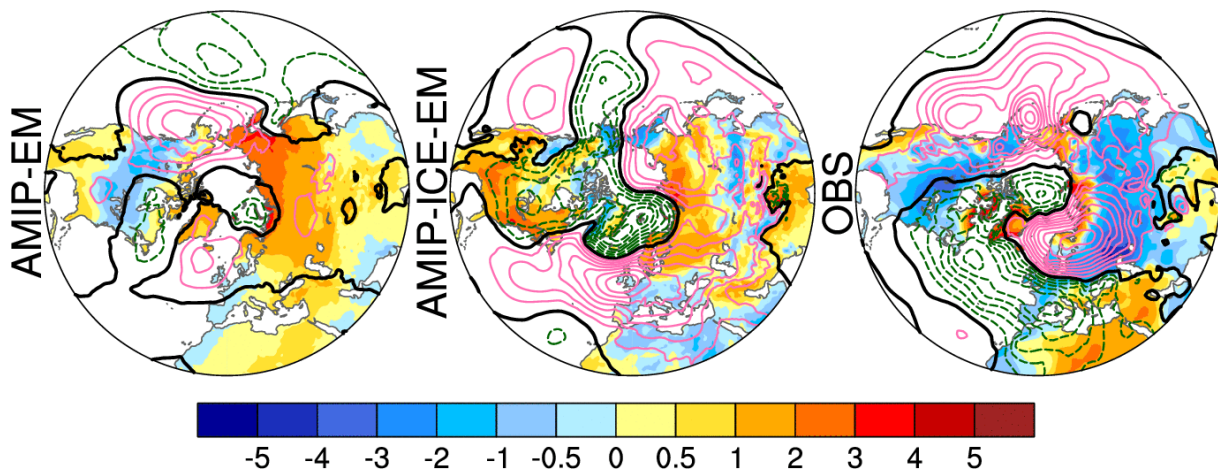


**Figure B.5:** as in Figure B.4 but for the HR version.



## Report from BSC/UB

Besides the dramatic “Arctic amplification”, i.e. surface air-temperature at polar latitudes rising twice as much as the global average, and the strong decline of Arctic sea-ice extent/thickness during recent decades, little is certain about their consequences and impact (Smith et al. 2019). Studies following a similar atmosphere-only, AMIP-like protocol as in WP5 of PRIMAVERA (see details in deliverable D5.1) have found that the role of Arctic sea-ice declining trends on long-term trends in the Northern Hemisphere atmospheric circulation or surface climate, for example the recent Eurasian cooling, is minimal (Perlitz et al. 2015; Ogawa et al. 2018), suggesting that some of the previously-reported signals (see Cohen et al. 2014 for review) were probably generated by internal variability (e.g. Sun et al. 2016); although there is still debate (e.g. Mori et al. 2019a, 2019b; Screen and Blackport 2019).

The (unrelated) question of whether sea-ice variability, around the long-term declining trends, might have or not a detectable influence on atmospheric variability has been much less explored in climate simulations (e.g. García-Serrano et al. 2017). The set-up of the atmosphere-only simulations in PRIMAVERA allows assessing that potential role. The comparison of the “control” experiment, with time-evolving SST and SIC variability over 1991-2014 under historical radiative forcings (hereafter AMIP), and the “sea-ice” experiment, similar to AMIP but with prescribed SIC climatology computed for 1979-1990 (hereafter CLIM), allows evaluating the influence of SIC variability on the atmospheric circulation. To reduce the effect of long-term nonlinear trends, all anomalies are cubically (3rd-order polynomial) detrended (see Fig. B.6).

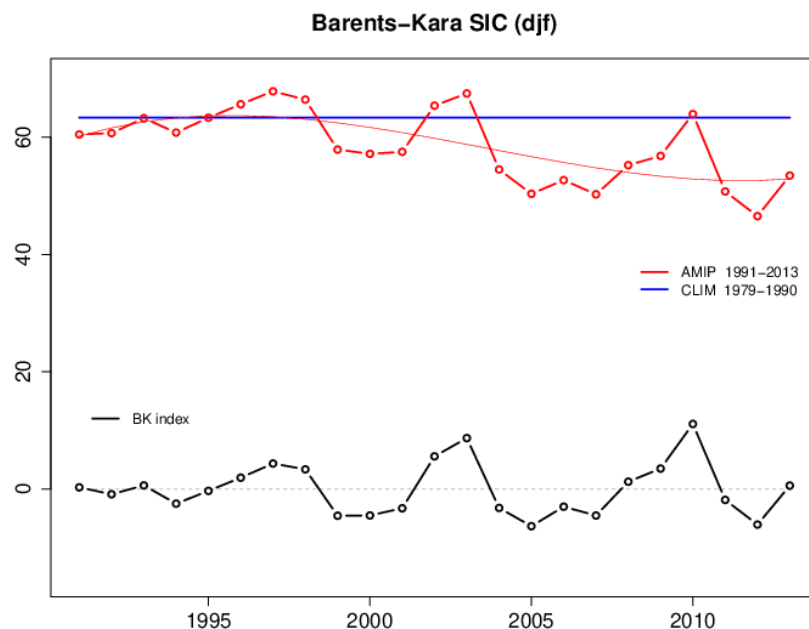


**Figure B.6** Illustration of sea-ice variability in the “control” (AMIP) and “sea-ice” (CLIM) experiments. Sea-ice concentration [%] averaged over the Barents-Kara Seas (10E-100E/70N-85N) in the forcing field of the AMIP (red) and CLIM (blue) experiments; overplotted in AMIP (thin red) is a 3rd-order polynomial fit, i.e. a cubic trend. Barents-Kara sea-ice concentration anomalies, after cubic detrending, is also shown (black). All time series are for the winter mean December-January-February.

Models contributing to the atmosphere-only WP5 experiments are: EC-Earth3P (Haarsma et al. 2020; hereafter EC-EARTH), with 10 members at both low resolution (LR, T255) and high

resolution (HR, T511); ECMWF-IFS cy43r1 (hereafter ECMWF), with 6 members at LR (Tco199) and 4 members at HR (Tco399); and, CNRM-CM6.1 (hereafter CERFACS), with 10 members at both LR (T127) and HR (T359). Note that the potential impact of sea-ice variability may well be model dependent (including resolution) and subseasonal, as it strongly depends on the mean-flow (see discussion in García-Serrano et al. 2017); so, no coherence in total variability among models or between LR and HR is *a-priori* expected.

Figures B.7-9 show changes in standard deviation of sea-level pressure (SLP) between AMIP and CLIM, at SR (left column) and HR (right column), for winter months: December (top), January (middle) and February (bottom); statistical significance is assessed with a Fisher's F-test for difference of variance. Regardless of model resolution, there appears that sea-ice variability has a stronger effect on SLP variability over the North Atlantic-Eurasian sector as compared to the North Pacific-American sector, with the exception of ECMWF for January (Fig. B.8-middle) that only shows signals in the latter and CERFACS at HR (Fig. B.9-right) that shows comparable changes in both regions.

The results suggest that increasing model resolution (HR vs LR) emphasizes the effect of sea-ice variability on SLP variability, with HR yielding significant and coherent changes in the three winter months, particularly for EC-EARTH and CERFACS, and to a lesser extent for ECMWF maybe due a smaller ensemble size. In particular, EC-EARTH HR shows more North Atlantic Oscillation (NAO)-like variability in AMIP than in CLIM for December (Fig. B.7b); less dipolar NAO-like variability, but more monopolar East Atlantic (EA)-like variability, for January (Fig. B.7d); and, finally, more Ural-Siberian variability in AMIP than in CLIM for February (Fig. B.7f). EC-EARTH LR shows only a large-scale impact in December, with a pattern depicting more NAO-like variability under sea-ice variability (Fig. B.7c). ECMWF HR shows more NAO-like variability over the North Atlantic for December (Fig. B.8b), and a dipolar pattern over the North Pacific for January (Fig. B.8d). Note that the effect of sea-ice variability on Ural-Siberian variability is opposite for December in ECMWF LR (Fig. B.8a), showing less variability, than in HR (Fig. B.8b), hinting at an increase of variability. Lastly, CERFACS HR yields a strong reduction of SLP variability over western North Atlantic-Europe for December (Fig. B.9b); and, more (less) NAO-like (EA-like) variability for both January (Fig. B.9d) and February (Fig. B.9f) in AMIP than in CLIM. Also, CERFACS HR has a clear impact on Ural-Siberian variability in early winter, displaying more variability for December (Fig. B.9b) and less variability for January (Fig. B.9d). Note that CERFACS HR shows a strong sensitivity of the Aleutian Low variability to sea-ice variability, which is not found in the other models. Concerning CERFACS LR, it yields less Ural-Siberian variability for December (Fig. B.9a), consistent with ECMWF LR (Fig. B.8a), and more SLP variability at North Atlantic high latitudes for January (Fig. B.9c), in agreement with EC-EARTH LR (Fig. B.7c).

A local feature that is robust in the three models, at both LR and HR, consists of an increase in SLP variability around Newfoundland for February, probably linked to a southern location of the sea-ice edge in this month; although it is statistically significant only for EC-EARTH (Fig. B.7e,f) and CERFACS (Fig. B.9e,f) not for ECMWF (Fig. B.8e,f) perhaps due to a smaller ensemble size.

As an example of the reported changes in SLP standard deviation, e.g. EC-EARTH HR (Fig. B.7-right), Fig. B.10 shows how sea-ice variability affects the fraction of explained variance of the leading SLP variability modes; in particular, the NAO and EA patterns over North Atlantic-Europe (Fig. B.10a-c), and the Ural-Siberian pattern over Eurasia (Fig. B.10d).

To conclude, these results imply that sea-ice variability can have a detectable influence on the large-scale atmospheric variability at mid-high latitudes in present climate, which

appears to be stronger in the North Atlantic-Eurasian sector and emphasized by high-resolution models.

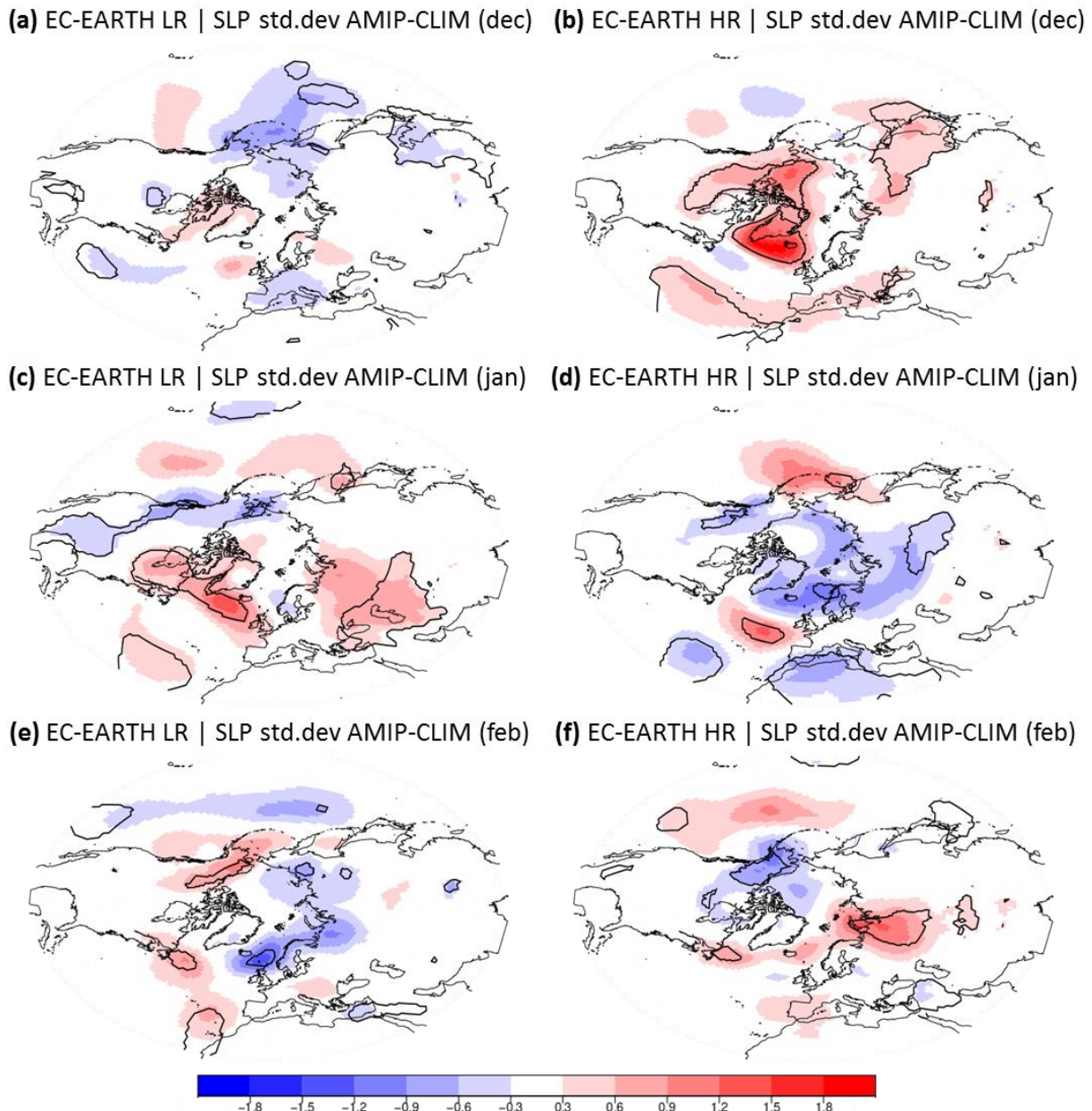


**Figure B.7.** Difference in standard deviation of cubically-detrended SLP anomalies between AMIP and CLIM in EC-EARTH at low resolution (LR, left) and high resolution (HR, right) for winter months: December (top), January (middle), and February (bottom). Total variability has been analysed concatenating the 10 members for 1991/92-2013/14 (23 winters). Statistically significant areas according to a Fisher's F-test at 95% confidence level are contoured.

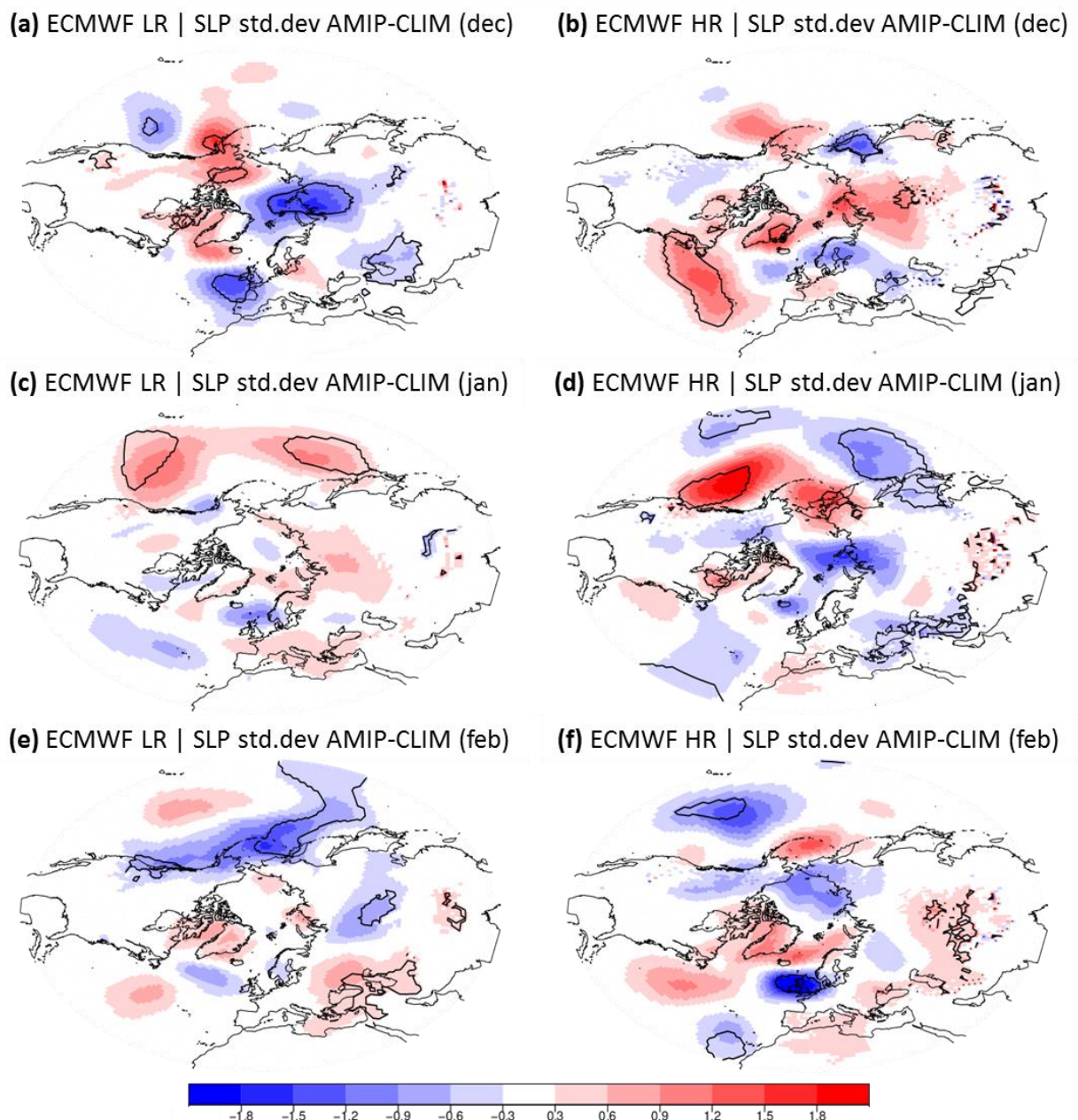


**Figure B.8.** As Fig. B.7, but for ECMWF; with 6 (4) members at LR (HR).

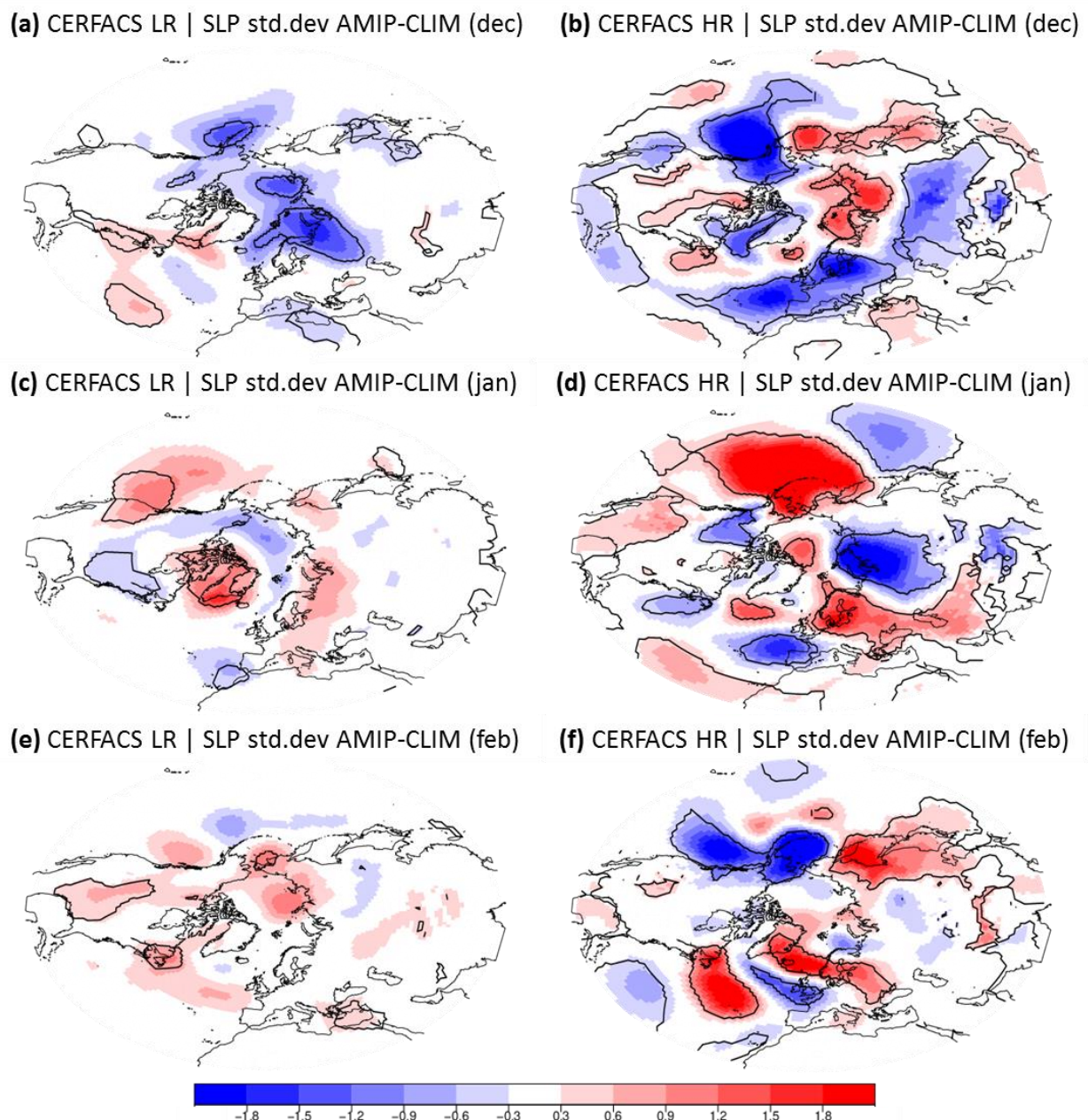


**Figure B.9.** As Fig. B.7, but for CERFACS; with 10 members at both LR and HR.

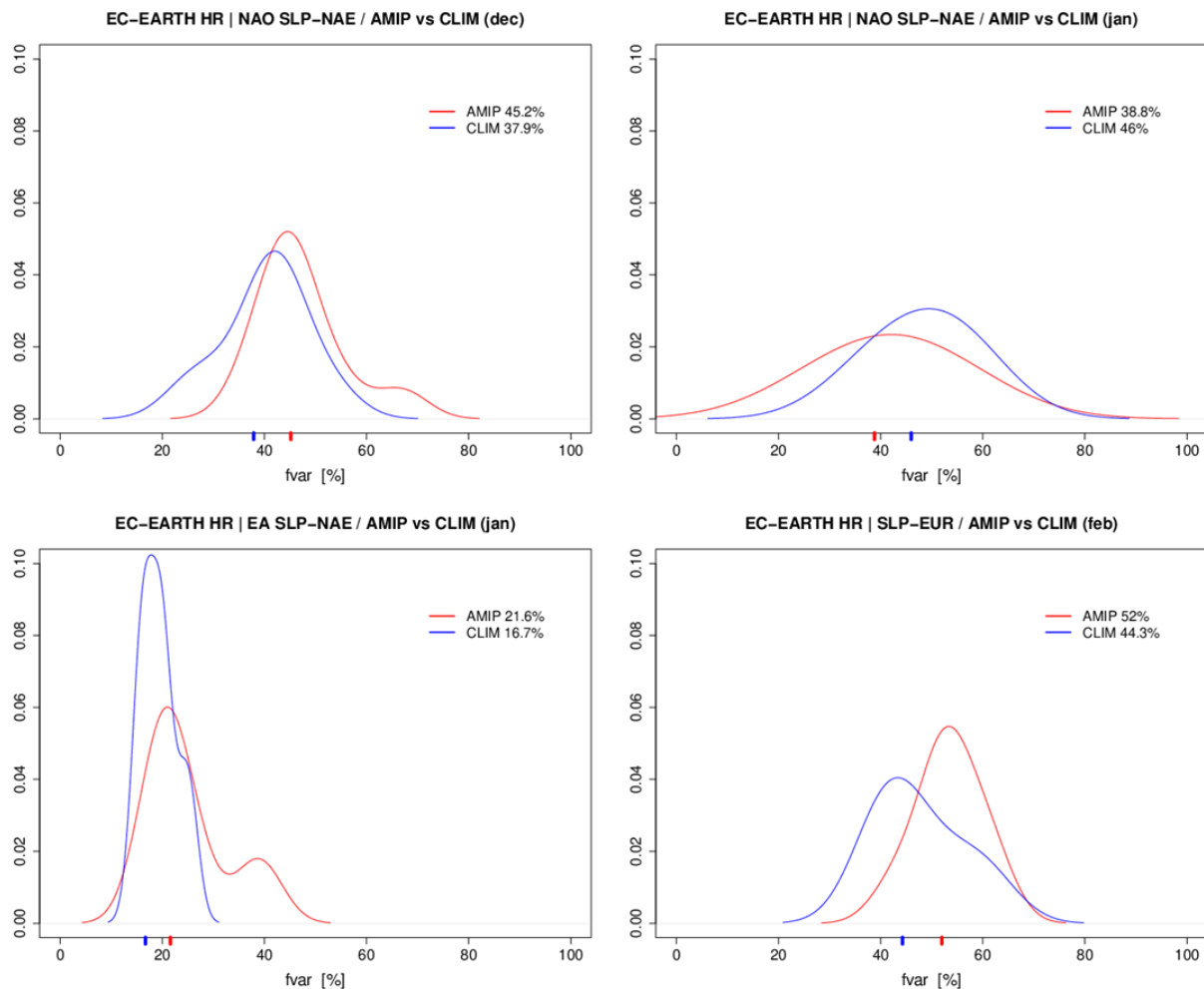


**Figure B.10.** Probability density function fitted with the fraction of explained variance of individual members from EOF analysis of cubically-detrended SLP anomalies over the North Atlantic-European region (NAE 90W-40E/20N-90N) and the Eurasian region (EUR 20E-140E/20N-90N) for winter months (see titles). The NAO (EA) pattern corresponds to the first (second) EOF over the NAE region, while the Ural-Siberian pattern corresponds to the first EOF over the EUR region. The ensemble EOF has been computed concatenating all members before analysis; the fraction of explained variance in the ensemble EOF is indicated in the legend and highlighted in the abscissa axis.

#### REFERENCES:

- Cohen, J. et al. (2014): Recent Arctic amplification and extreme mid-latitude weather. *Nature Geosci.*, 7, 627-637.
- García-Serrano, J., C. Frankignoul, M.P. King, A. Arribas, Y. Gao, V. Guemas, D. Matei, R. Msadek, W. Park, E. Sanchez-Gomez (2017): Multi-model assessment of linkages between eastern Arctic sea-ice variability and the Euro-Atlantic atmospheric circulation in current climate. *Clim. Dyn.*, 49, 2407-2429.
- Haarsma, R.J., et al. (2020): HighResMIP versions of EC-Earth: EC-Earth3P and EC-Earth3P-HR. Description, model computational performance and initial validation. *Geosci. Model Dev.* (under review).
- Mori, M., Y. Kosaka, M. Watanabe, H. Nakamura, M. Kimoto (2019a): A reconciled estimate of the influence of Arctic sea-ice loss on recent Eurasian cooling. *Nature Clim. Change*, 9, 123-129.

Mori, M., Y. Kosaka, M. Watanabe, B. Taguchi, H. Nakamura, M. Kimoto (2019b): Reply to 'Is sea-ice-driven Eurasian cooling too weak in models?'. *Nature Clim. Change*, 9, 937-939.

Ogawa, F., N. Keenlyside, Y. Gao, T. Koenigk, S. Yang, L. Suo, T. Wang, G. Gastineau, T. Nakamura, H.N. Cheung, N.-E. Omrani, J. Ukita, V. Semenov (2018): Evaluating impacts of recent Arctic sea ice loss on the Northern Hemisphere winter climate change. *Geophys. Res. Lett.*, 45, 3255-3263.

Perlitz, J., M. Hoerling, R. Dole (2015): Arctic tropospheric warming: causes and linkages to lower latitudes. *J. Clim.*, 28, 2154-2167.

Screen, J.A., R. Blackport (2019): Is sea-ice-driven Eurasian cooling too weak in models?. *Nature Clim. Change*, 9, 934-936.

Smith, D.M. et al. (2019): The Polar Amplification Model Intercomparison Project (PAMIP) contribution to CMIP6: investigating the causes and consequences of polar amplification. *Geosci. Model Dev.*, 12, 1139-1164.

Sun, L., J. Perlitz, M. Hoerling (2016): What caused the recent "warm Arctic, cold continents" trend pattern in winter temperatures?. *Geophys. Res. Lett.*, 43, 5345-5352.

## Report from SMHI

We analyse the response to a change in Arctic sea ice over a period of 24 years (1991-2014) in five experiments using two global uncoupled models. All experiments are initialised from a 1950 control experiment and daily sea ice concentration (SIC) is prescribed corresponding to a climatologically cooler period (1979-1990) and a warmer period (2005-2015) to analyse the response to an increase and decrease in sea ice, respectively. The experiments are run at standard and high resolution by each modelling centre; the details of which are given in Table B.1. Experiments at SMHI and BSC use the EC-Earth3 model at standard resolution (T255L91, ~100 km) and high resolution (T511L91, ~50 km), and experiments at ECMWF use the IFS model (CY43R1) at standard (Tco199L91, ~50 km) and high resolution (Tco399L91, ~25 km). All the experiments use 91 vertical levels.

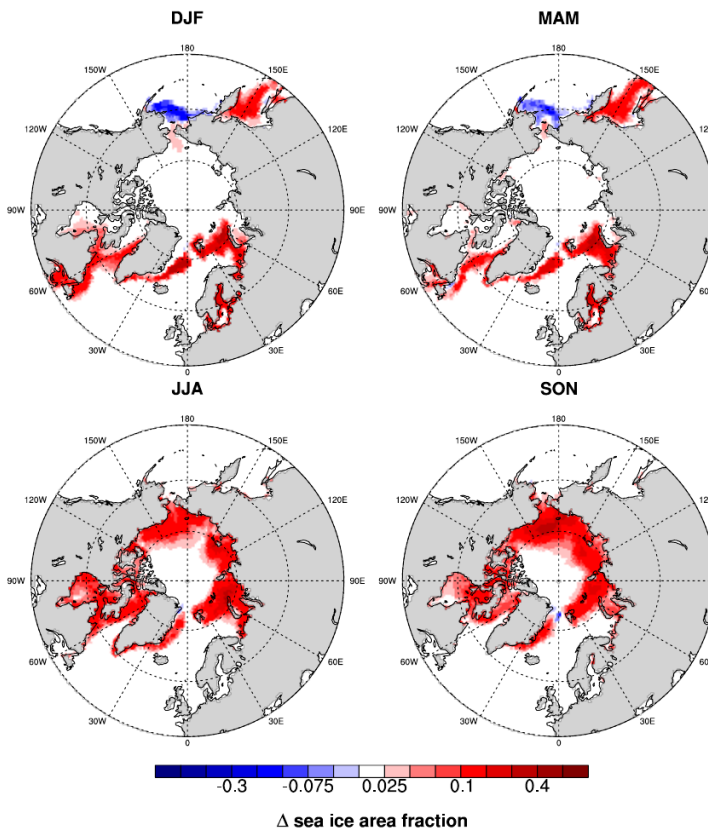
<b>Experiment name</b>	<b>Centre</b>	<b>Resolution</b>	<b>Number of ensemble members</b>	<b>Change in sea ice area</b>
S SR	SMHI	T255L91	11	increase
S HR	SMHI+BSC	T511L91	10	increase
E SR	ECMWF	Tco199L91	6	increase
E HR	ECMWF	Tco399L91	4	increase
S 2	SMHI	T255L91	11	decrease

Table B.1: An overview of the experiments conducted.

The results presented here use the mean of all the ensemble members taken from monthly mean output.

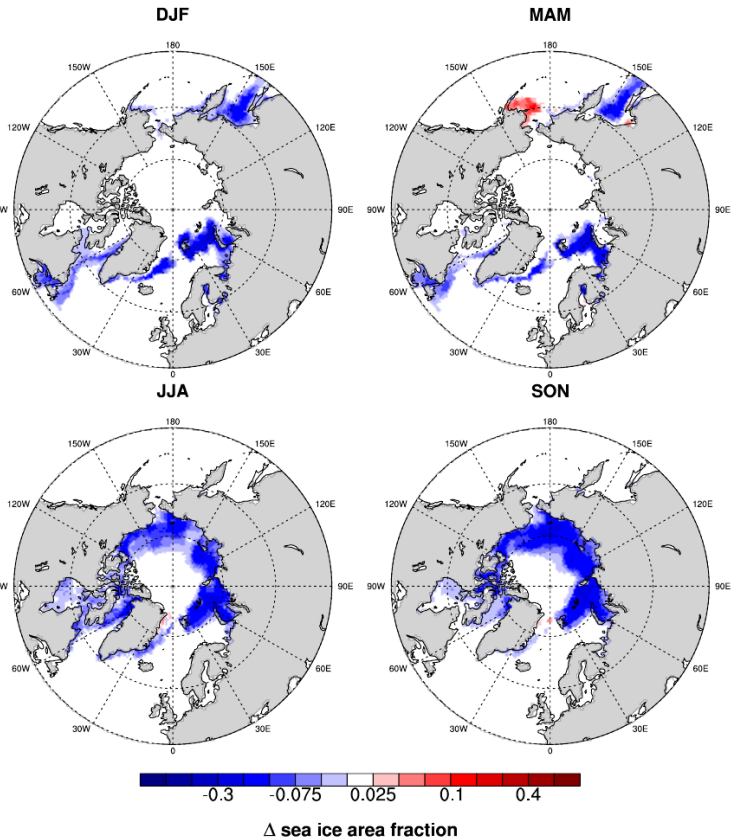
The spatial distribution of the seasonal mean change in Arctic sea ice area fraction prescribed over the period analysed (1991-2014) is shown in Figure B.11, for both the climatologically cool and warm period.

Sea ice area fraction (S SR - CTL) 1991-2014



a)

Sea ice area fraction (S 2 - CTL) 1991-2014



b)

Figure B.11: Seasonal mean change in prescribed sea ice area fraction for a) increased sea ice experiments and b) decreased sea ice experiments.

In the experiments where sea ice area is increased, a near-surface cooling is seen during all seasons closely following areas of increased SIC (Fig.B.12). The greatest cooling is seen in autumn and winter, with a mean decrease of  $-1.5^{\circ}\text{C}$  over regions with increased sea ice (with an increase in SIC of at least 0.025%) in S SR. A slight cooling is seen beyond these regions, in Eurasia, although it is not statistically significant. Doubling the resolution (S HR) increases the area of cooling over Eurasia slightly, although the mean change remains consistent with the standard resolution experiment (Figs. B.12 and B.15a). The ECMWF IFS experiments display similar mean temperature change statistics as the EC-Earth experiments (Fig. B.15a), although during winter a slight cooling is seen over wider regions of Eurasia and North America (not shown). These changes are not statistically significant, however.

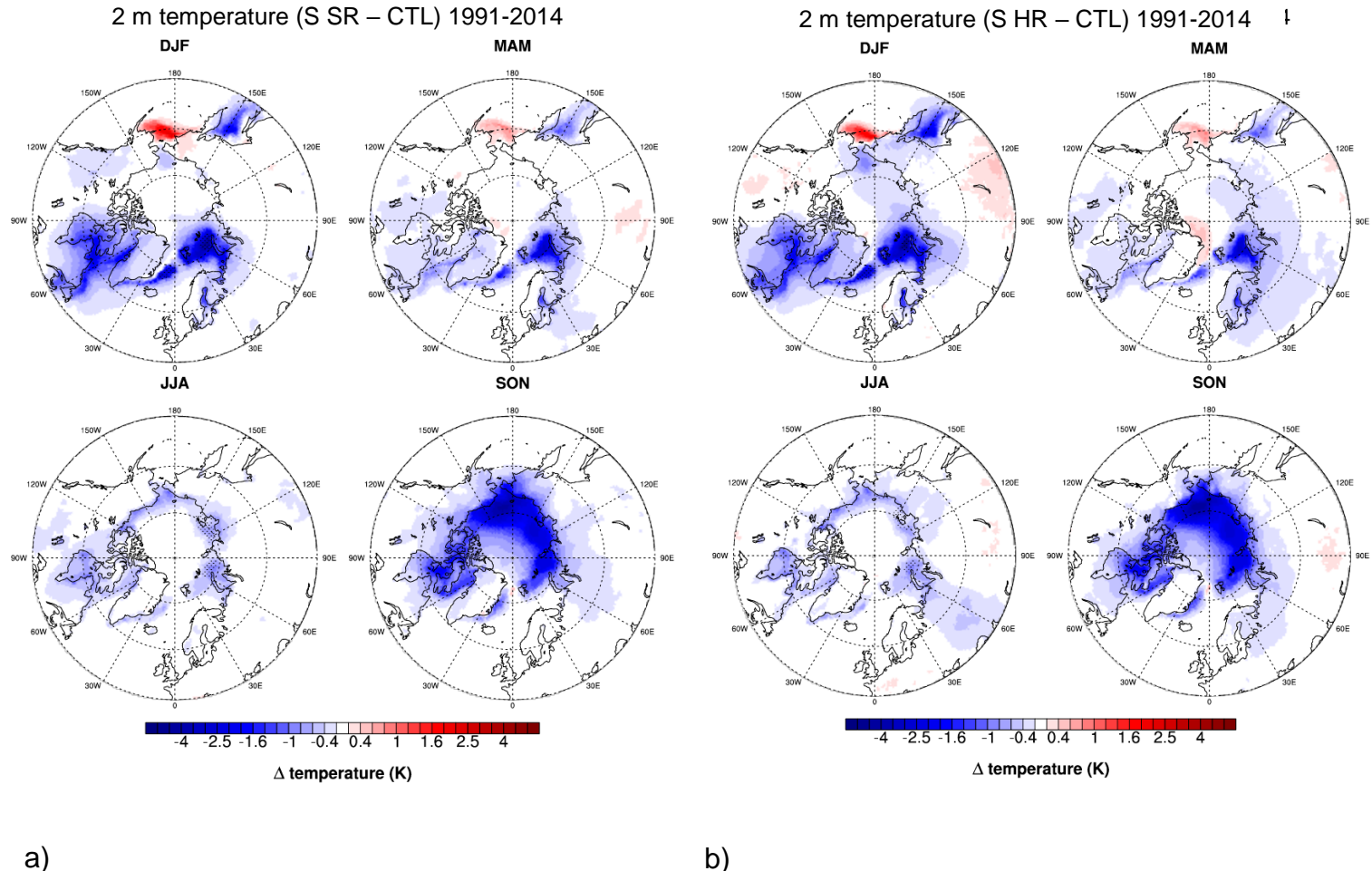


Figure B.12: Seasonal mean 2 m temperature change for EC-Earth3 increased sea ice experiments, for a) standard resolution (S SR) and b) high resolution (S HR). Dotted areas denote statistical significance at the 5% level using a two-sided Student t-test.

2 m temperature (S 2 – CTL) 1991-2014

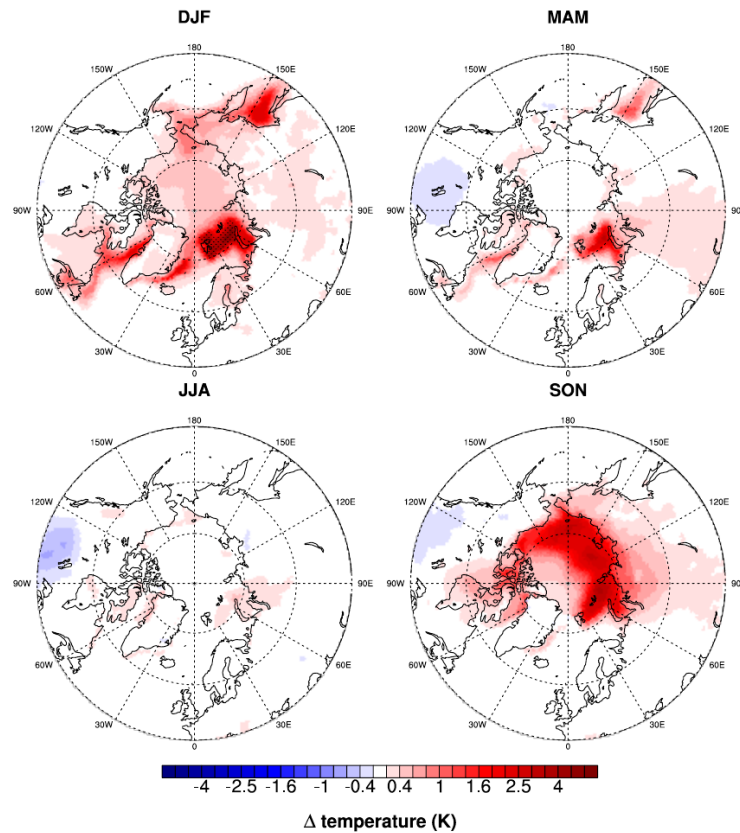


Figure B.13: Seasonal mean 2 m temperature change for the EC-Earth3 decreased sea ice experiment (S 2). Dotted areas denote statistical significance at the 5% level using a two-sided Student t-test.

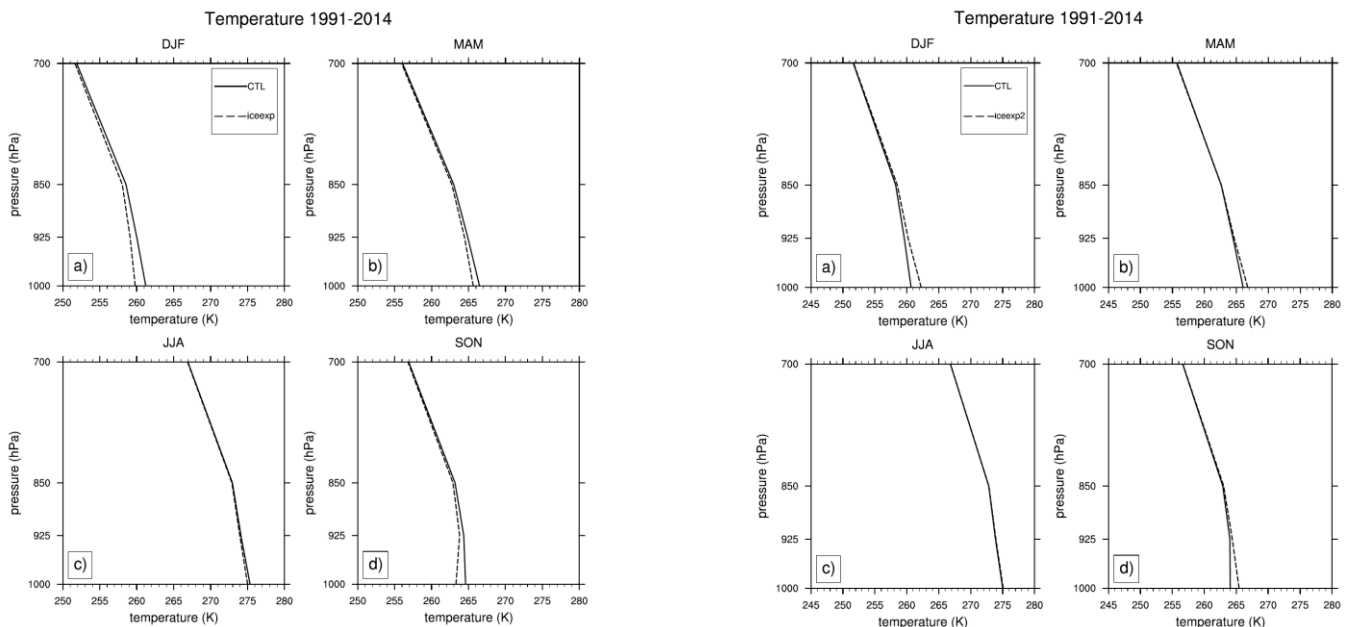


Figure B.14: Vertical mean profiles of temperature over regions with an increase in SIC (LHS) and a decrease in SIC of at least 0.025% (RHS), respectively. Regions south of 60°N are excluded. The solid lines denote the control experiment, and the dotted lines the experiment.

For the reduced sea ice area experiment (S 2), a warming in near-surface temperature is seen over areas of reduced SIC during all seasons (Fig. B.13). The greatest warming is seen during winter, with a mean increase of 1.7°C over regions with decreased sea ice (with a decrease in SIC of at least 0.025%). A slight warming is seen during winter over the whole of the Arctic Ocean and parts of Eurasia during spring, autumn and winter, although it is not statistically significant. Minimal changes are seen during summer. Temperature changes in all experiments remain limited in vertical extent to mostly below 850 hPa (Fig. B.14). Increasing the horizontal resolution has a very small impact on the vertical mean profile of temperature change (not shown).

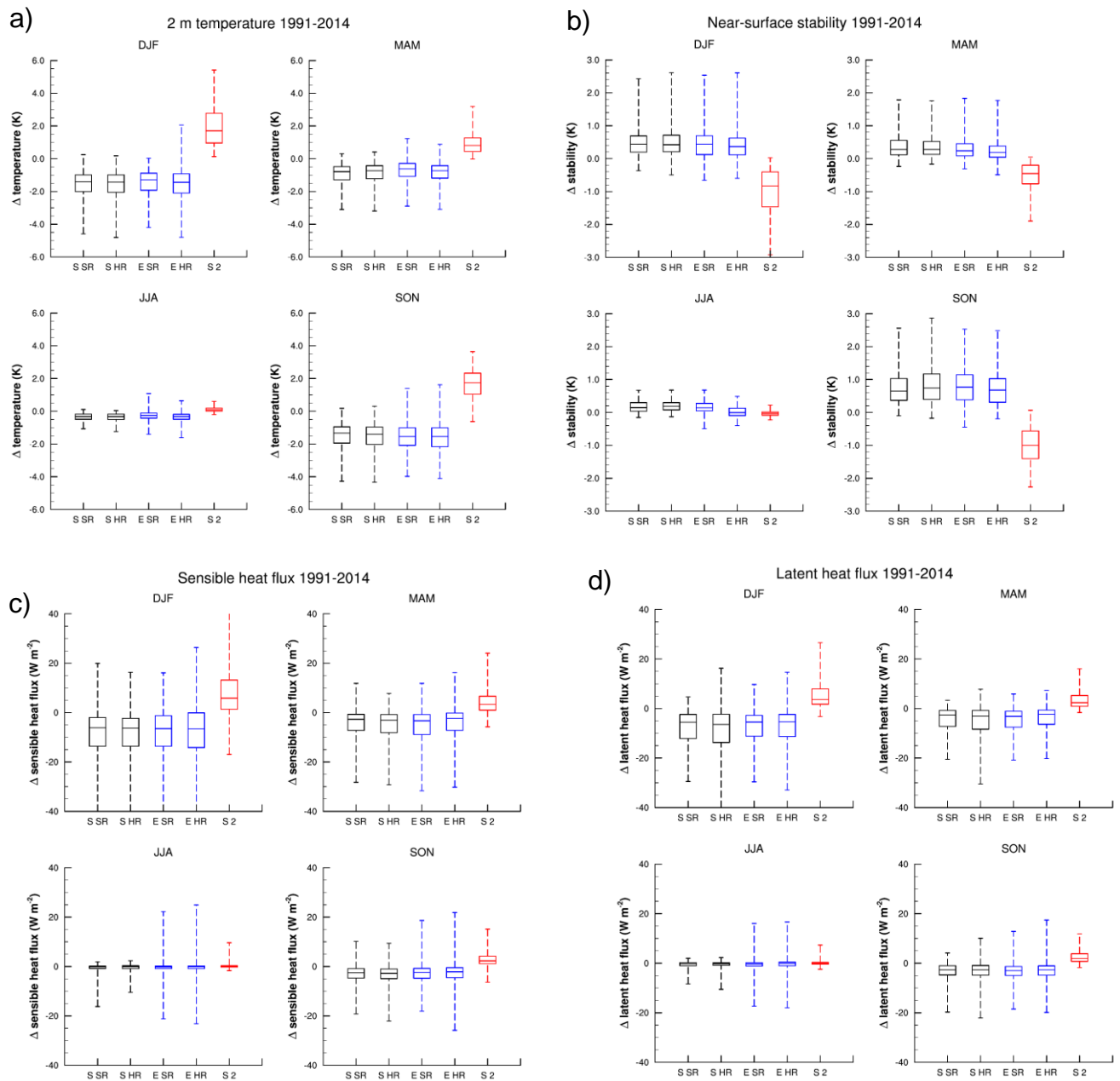


Figure B.15: Box plots of the mean difference over regions with sea ice area change (defined as a change of at least 0.025% north of  $60^{\circ}\text{N}$ , for a) 2 m temperature, b) near-surface static stability (defined as the difference in potential temperature between 925-1000 hPa), c) sensible heat flux and d) latent heat flux. The minimum, first quartile, median, third quartile and maximum values are indicated.

Sensible and latent heat fluxes increase during all seasons apart from summer (Fig. B.15c,d), with the greatest increase in winter of  $7 \text{ W m}^{-2}$  in sensible heat flux on average over regions with reduced sea ice. These fluxes result from changes in the air-sea temperature gradient. During summer, these gradients are small which suppress turbulent fluxes and have little impact on the near-surface static stability (Fig. B.15b). However, when the Sun sets in the autumn the air-sea temperature

gradient increases more over regions with less sea ice (owing to the difference in specific heat capacity between the ocean and air), resulting in an increase in the turbulent fluxes and a reduction in the near-surface stability (Fig. B.15). In the experiments where sea ice area increases, the air-sea temperature gradient is reduced, reducing the turbulent fluxes and increasing the near-surface static stability (Fig. B.15).

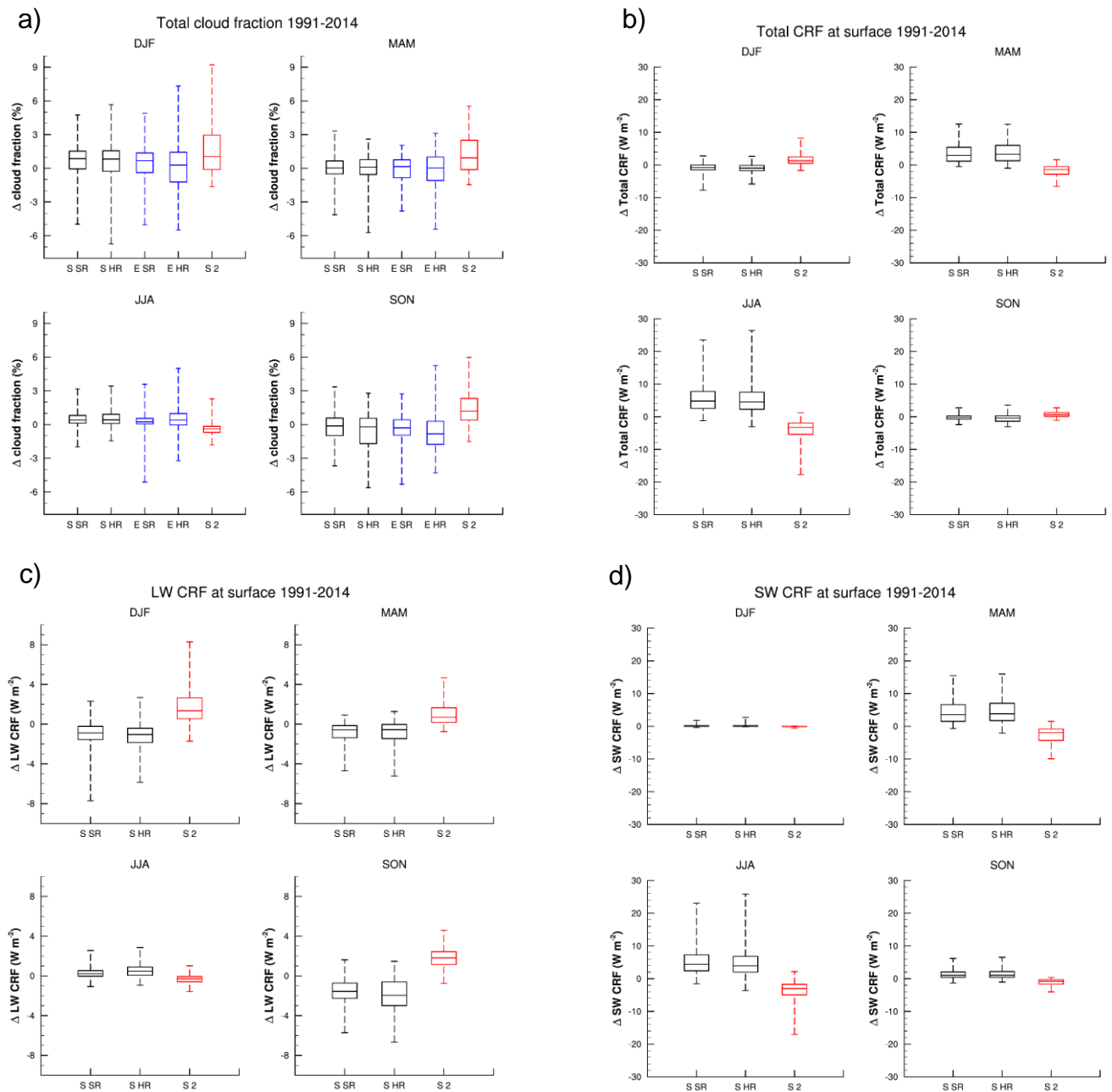


Figure B.16: As for Fig.B.15, for a) total cloud fraction, b) total CRF at surface, c) LW CRF at surface, and d) SW CRF at surface.

The increase in turbulent fluxes and corresponding decrease in near-surface stability during autumn, winter and spring in the reduced sea ice experiment results in a small increase in cloud fraction over regions with reduced sea ice (Fig. B.16a). A mean

increase of 1.5% is seen during the winter. As a result of the increase in cloud, an increase in longwave cloud radiative forcing at the surface (LW CRF) is also seen, with a mean increase of  $1.6 \text{ W m}^{-2}$  in autumn. In the increased sea ice experiments, the LW CRF is decreased slightly during all months apart from summer (where the change is very small). A maximum mean decrease of  $-1.5 \text{ W m}^{-2}$  is seen during autumn. The high resolution experiment (S HR) displays similar statistics as the standard resolution experiment (S SR), although there is greater spatial variability in autumn (Fig. B.16c).

For the SW CRF, the changes are small for all experiments during autumn and winter due to polar darkness. During spring and summer, the SW CRF is reduced in the experiment with reduced sea ice, by  $-3.5 \text{ W m}^{-2}$  on average during summer. The increased sea ice experiments display the opposite, with an increased SW CRF of  $5 \text{ W m}^{-2}$  on average in summer. The total CRF (SW + LW) at the surface is largely unchanged during autumn and winter (Fig. B.16b), apart from the reduced sea ice experiment (S 2), which has a mean increase of  $1.5 \text{ W m}^{-2}$  during winter. During spring and summer the total CRF is reduced in this experiment, by  $-4 \text{ W m}^{-2}$  on average in summer. The opposite is true for the increased sea ice experiments, with a mean increase in total CRF of  $5.6 \text{ W m}^{-2}$  in summer (S SR). Increasing the resolution (S HR) has little impact on the total CRF (Fig. B.16b).

Statistically significant changes were not seen in the seasonal or monthly means for pressure, wind and precipitation, and are not discussed further here. The number of ensemble members would need to be increased to see a robust signal in these variables.

## Appendix C: Results from snow cover reduction experiments

### Report from SMHI

#### C.1. Introduction

Snow cover is one of the most important components of the cryosphere and roughly 98% of seasonal snow cover lays in the North Hemisphere (Armstrong, 2001). The mean maximum area extent is about 47 million square kilometers in winter (Robinson, 1993). It has long been understood that snow cover variability has strong seasonal distinctions, particularly accounts for the large differences between winter and summer. Satellite records indicate that snow cover has significantly decreased in spring during the past few decades and the largest changes occurred in June (IPCC, 2013), while during fall to middle winter, snow extent has remained relatively constant since the middle of 1980s (Robinson, 2010).

Snow cover plays a crucial role in regulating climate due to its optical properties. It reduces the solar radiation absorption and strongly influences the global energy balance due to its strong reflectivity and lower thermal diffusivities (Jones, 2001, Gong, 2004). Snow cover insulates the ground surface and weakens the moisture exchanges between the atmosphere and land surface. This further affects the terrestrial water balance (Derkson, 2000).

Previous studies reveal that snow over land triggers the direct local spatial and temporal climate variability (Brown and Robinson, 2011; Peings, 2011). Extent of snow cover is expected to feedback to temperature trends, particularly over Eurasian (Peng, 2013). Changes in the snow cover phenology led to contrasting anomalies of snow radiative forcing due to earlier snow end date and these snow feedbacks to air temperature are more robust in spring (Chen, 2015). Meanwhile, snow cover also exhibits indirect remote and continental-scale atmospheric circulation response (Peings, 2010; Handorf, 2015). Based on observational evidence, a significant snow-AO (Arctic Oscillation) link is detected (Cohen, 1999). It motivates into research how snow cover reduction may impact high and mid-latitude climate.

In the past decades, numerous numerical studies have been performed to investigate the local response and the teleconnection between snow cover and large-scale circulation with general circulation models (GCMs). However, the climate model cannot capture the observed snow–AO relationship (Furtado, 2015). Although model details can control the persistence and amplitude of the response to the snow forcing, the robust aspects of the simulated response do not always correspond to observed circulation anomalies associated with prescribed snow forcing (Fetcher, 2009). Sensitivity experiments with prescribed snow cover anomaly usually illustrated a much weaker snow–circulation linkage. This may be related to the unrealistic representation of stratospheric dynamics (Hardiman, 2008; Fetcher, 2009). Fetcher (2009) found that the well-resolved stratosphere exhibits a faster and weaker response to snow forcing. Peings, et al. (2012) used a nudging methodology to obtain a more realistic representation of the polar vortex and they found that correct representation of the stratospheric mean state can help to capture the observed snow–AO teleconnection.

Although models usually only poorly capture the snow-AO linkage, some models also show that the internal variability may play a significant role in the observed relationship (Furtado, 2015). Previous studies mainly concentrated on the impact snow cover anomalies during certain seasons over some key snow regions. In this study, we try to shed light on the snow cover impact from a different angle. Since snow cover is not explicitly described in the model and the close dependence between snow cover and snow albedo are supported by

satellite observations (Allen, 2011), we decided to reduce the snow albedo to produce snow anomalies in a physically consistent way, which give us the possibility to study the snow feedback mechanism. Simultaneously, taking into account the impact of internal variability, continuing long period integration will be performed.

## C.2 Experiments design

Previous studies have used GCMs to investigate the possible atmosphere feedback due to anomalous snow cover. To force such an anomalous snow cover scenario, snow conditions (snow cover, snow depth or snow water equivalent) are prescribed and treated as surface boundary conditions. Lacking feedback from atmosphere to snow cover, the non-linear interaction between the land surface and atmosphere could be weakened. In EC-Earth model, snow cover is not implicitly described in the snow model. As snow cover variability causes significant changes in surface albedo and consequently affects surface energy budget. Here we adapt an idea to set surface albedo to a constant value. This allows us to investigate the potential climatic response due to freely evolving snow conditions.

In this study, we have performed simulations using Ec-earth model with standard resolution (T255) and high resolution (T511) and designed one control experiment and two snow albedo reduction experiments for each resolution. All experiments were done over the period 1980-2015, which comprised 11 ensemble members for T255 and 5 ensembles for T511. All experiments start from initial conditions in 1980 that were taken from a previous spin-up simulation and are forced with daily SST and SIC datasets that have been prepared for the PRIMAVERA project based on HadISST2 dataset. Each ensemble member starts from a slightly different initial state. In order to get a robust signal, we specify snow albedo to 0.3 for all sensitivity experiments. This will create a strong year-around snow cover reduction, instead of focus on specific months or seasons. In the first set sensitivity experiments, the snow albedo is reduced over the whole North Hemisphere. To further identify the Eurasia climate response to Eurasia snow cover forcing, particularly over Siberia, the snow albedo is only reduced over Eurasia region ( $30^{\circ}\text{N}$ - $90^{\circ}\text{N}$ ,  $0^{\circ}\text{E}$ - $180^{\circ}\text{E}$ ) in the second set sensitivity experiments.

Fig. C.1 shows the annual cycle of snow cover extent over Eurasian in the control and sensitivity experiments for T255. Compared to control run, snow cover has been systematically reduced in the whole year-around, largest decreases are in winter and spring. Another distinct feature is that the snow cover has completely disappeared in the summer. High resolution simulations show very similar snow cover extent seasonal cycles (figures not shown). Apart from assessing response of the North hemisphere atmospheric circulation and the sensitivity of Eurasian climate to snow cover variability, these experiments will also allow us to investigate the impact of horizontal resolution on European climate.

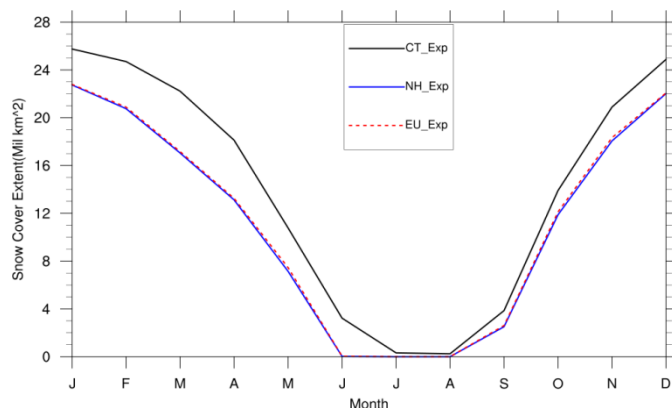


Fig. C.1 Annual cycle of snow cover extent over Eurasia ( $35^{\circ}\text{N}$ - $70^{\circ}\text{N}$ ,  $30^{\circ}\text{E}$ - $150^{\circ}\text{E}$ ) in control run(CT\_Exp), North Hemisphere Experiment (NH\_Exp) and Eurasian Experiment (EU\_Exp) for at T255 resolution.

### C.3 Results from North Hemisphere snow albedo reduction experiment

#### C.3.1 Surface response

Previous snow cover experiments usually focus on specific seasons with prescribed surface boundary conditions. Here in our experiments, snow cover extent is reduced year-around due to a fixed low snow albedo (Fig. C.1). This motivates us first to investigate the seasonal responses due to snow cover inter-annual variation. Figure C.2 shows the ensemble mean seasonal surface temperature differences between North Hemisphere snow albedo reduction experiments and control experiments in spring, summer, autumn and winter, respectively for T255 and T511 resolutions. Dotted areas are statistically significant at the 95% confidence level based on a two-sided Student's t test. Since reduced snow cover albedo leads to earlier snow melting and this weakening albedo effect contributes to direct surface heating. However, the terrestrial surface air temperature responses are not only confined over snow cover regions. Firstly we focus on T255 resolution experiments, seen from Fig. C.2 , the air temperature responses show strong warm biases over the whole Eurasian continent for all seasons. Moreover, magnitude of responses illustrate different seasonal dependence. In spring, maximum temperature responses exceeding 3K is adjacent to the Arctic coast over the northern part of the continent. Significant strong warm anomalies are also found over central of Eurasian and the Tibet Plateau. In summer, large warm biases mainly occur over central Siberia along the Arctic coast. As illustrated in Fig. C.1, snow cover completely disappears during summer in snow reduction experiments, but the sea ice cover is prescribed in our experiments. Therefore, the differential melting of snow cover and sea ice cover along Siberian coast results in a strong temperature gradient. In autumn, the spatial distribution pattern resembles spring which might due to that autumn and spring are both transitional seasons between winter and summer. Weaker snow albedo results in less number of snow days and less snow cover extent, particularly in high latitude regions. A smaller snow cover extent reduction in autumn (Fig. C.1) has contributed to a much weaker response. The magnitude of warm biases has decreased about 1K compared to spring response. Winter is the dominant snow season in the Northern Hemisphere. Due to shorter day-time in the high latitude region, this indicates that the effect of snow albedo is weakened compared to the middle-latitude region. The warm biases larger than 3K extend from the central of Eurasian to the Tibet Plateau. Compared with T255 simulations, there are no significant differences for all seasons in T511 experiments. It is only about 0.5K warmer in part of eastern Eurasian.

Another snow effect is snow-hydrological effect. The snow melting will change the soil moisture and exhibits a strong land-atmosphere coupling between evaporation and precipitation. Considering the lag-effect of soil moisture due to climate memory, this has particularly robust effects in summer (Matsumura, 2012). Fig. C.3 illustrates the response of precipitation between North Hemisphere snow albedo reduction experiments and control experiments. In T255 experiments, the spatial distribution of precipitation relative change in spring is characterized by isolated wetting maxima over eastern Siberian and the Tibet Plateau and drying maxima over central of Eurasian. Over eastern Siberian and the Tibet Plateau the precipitation differences are coincident with the surface air temperature differences (Fig. C.2). The melting snow due to warmer temperature leads to wetter soil moisture. This indicates that the increased precipitation over these regions largely contributed from local evaporation. The spatial pattern of total cloud cover in spring also

shows a close resemblance to surface air temperature changes (figures not shown). This confirms the dominant role of surface air temperature in the snow melting process. However, in spring only minor snow cover is in the south of 50°N over central of Eurasian. The warmer air temperature enhances the soil moisture deficit and results in less precipitation. In summer lower snow albedo leads to free snow over Eurasian except the Tibet region. Over eastern Siberian, the increased precipitation is mainly due to enhanced soil moisture from spring. Matsumura (2010) pointed out that the spring snow cover variation over Eurasian closely related to summertime atmospheric and hydrological circulation. From west Europe to central Eurasian, striking continental-wide negative precipitation changes are seen over the mid-latitude region (south of 50°N). Similar to spring, strong surface heating leads to drier soil moisture over this region. In autumn, noticeable precipitation decreasing is seen over south and east of the Caspian Sea which are desert or semi-desert regions. In direct contrast, precipitation increasing is seen over the Tibet region. Similar spatial distribution is seen in winter, however, more significant precipitation increasing is seen over Easter Siberian and China. In T511 experiments, the spatial patterns of precipitation response resemble T255 experiments. In spring and summer, the dry-and-wet contrast patterns between west and East Eurasian are slightly enhanced. This implies that high resolution tends to have a stronger snow-hydrological effect.

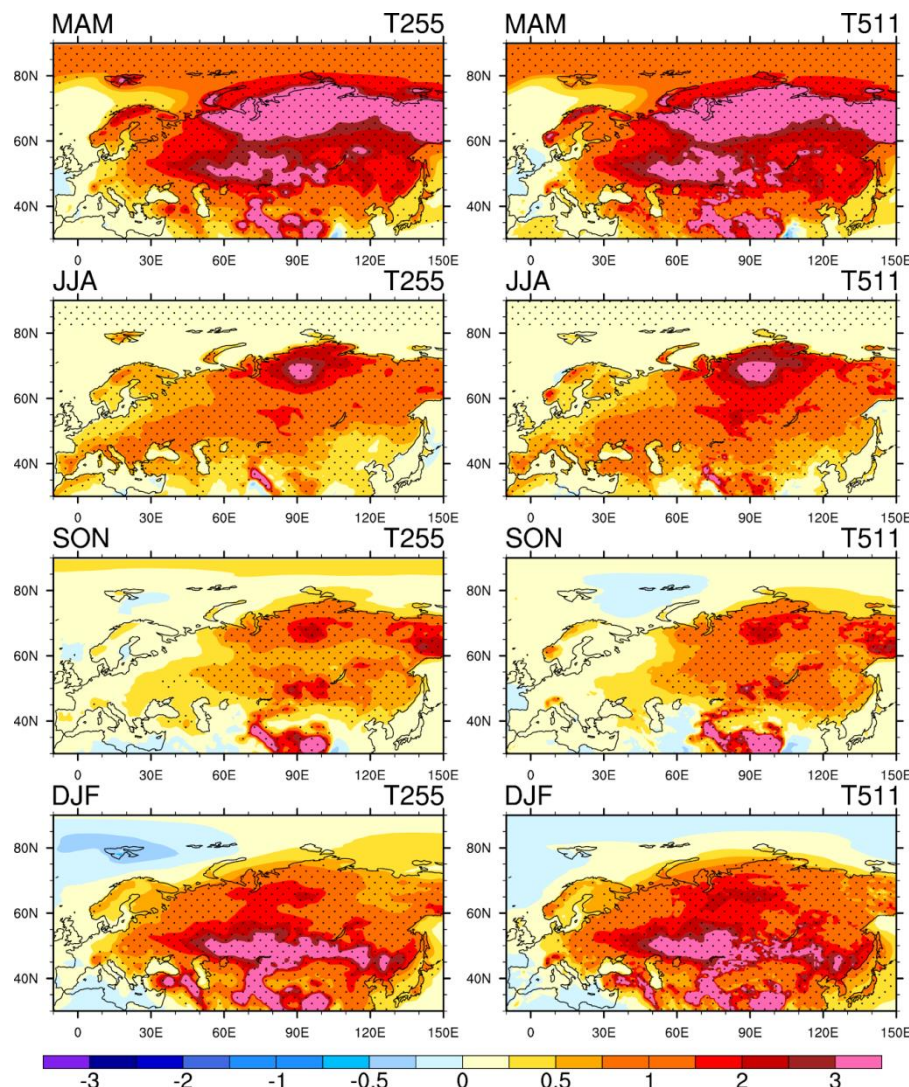


Fig. C.2 Ensemble Mean surface air temperature differences between North Hemisphere experiment and control experiment for MAM, JJA, SON and DJF (Dotted area denotes significant values except 95% confidence level based on a Student's t-test) in T255(Left) and T511 (Right) resolutions

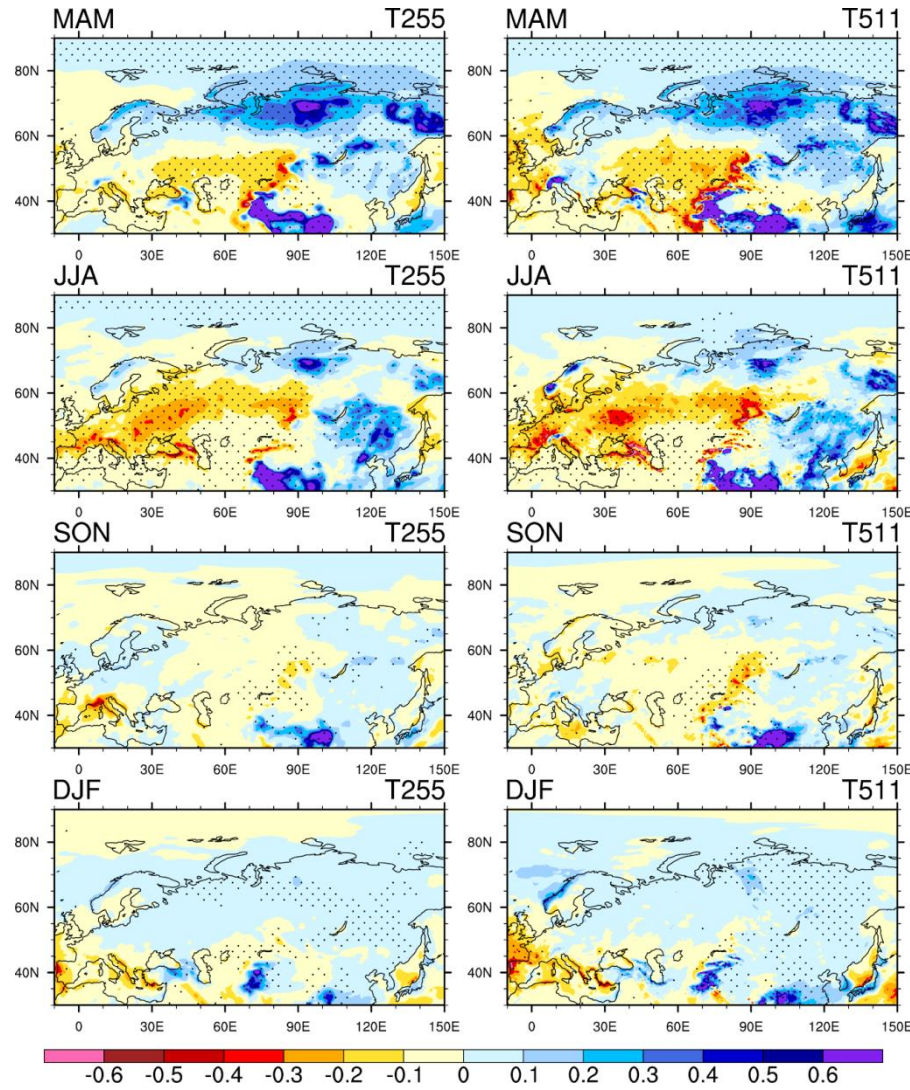


Fig. C.3 Same as Fig. C.2 but for mean precipitation (unit:mm/day)

As we know surface temperatures are closely related to the surface energy balances. The altering of surface energy components will contribute to the surface air temperature warming through different processes. In our experiments, the dominant effect of reduced snow albedo causes a strong radiative warming at the underlying surface. This will directly alter the turbulent fluxes (sensible and latent heat fluxes), which are dominant terms in the surface energy budget. Figs. 4 and 5 illustrate the relative changes of ensemble mean sensible and latent heat fluxes between North Hemisphere snow albedo reduction experiments and control experiments (positive downward). In T255 experiment, the sensible heat flux response in spring (Fig. C.4) is considerably large and the maximum response (the amplitude is about  $-15\text{wm}^2$ ) coincides with the warmest temperature response (Fig. C.2). These regions are mainly localized to snow cover reducing regions, the insulating effect of snow is weakened or disappeared, which is associated with increased short wave radiation absorption and emitted thermal radiation partially balanced the enhanced surface heating (figures not shown). In the northern Eurasian, latent heat fluxes (Fig. C.5) also shows equivalent heat loss into the air as the sensible heat fluxes, which is due to the increased

soil moisture and local precipitation. Vice versa, the latent heat flux shows an opposite response over the southern Eurasian (south of 50°N) excluding the Tibet Plateau. In spring there is little snow cover over these regions and decreased precipitation corresponds to drier soil moisture, this suggests that the warm surface response over this region is mainly via the sensible heat flux. The enhanced net short wave energy fluxes is also a factor (Figure not shown). In summer, both sensible and latent heat fluxes (Fig. C.4 and 5) show similar spatial patterns as in spring, respectively. The magnitude of atmospheric received sensible heat flux is much smaller compared to spring over the whole Eurasian. Since the snow cover almost completely disappears in summer, the robust outgoing latent heat flux is mainly in the Siberian region due to snowmelt. Over the southern Eurasian, drier continent climate leads more enhanced latent heat fluxes. The reduced total cloud cover also plays an important role (figure not shown). In autumn, although there are still strong warm atmospheric responses (Fig. C.2), both sensible and latent fluxes show very small variation across the whole Eurasian excluding the Tibet Plateau. As snow cover is mainly in the high latitude or elevation regions during autumn, temperature warming over these regions are due to enhanced solar radiation. During winter, only sensible heat fluxes show an evident response over southern Eurasian (Fig. C.4). Reduced snow albedo exhibits both snow cover and snow depth variability. Over high latitude regions, snow cover variability is minor, but this may link with extensive snow depth variability. This shallow snow cover leads to weaker contribution to local atmospheric warming (Baker, 1992; Fallot, 1997). However, over southern Eurasian, lower snow albedo leads to snow free regions and this exhibits a stronger local warming response. Both solar radiation and long-wave radiation fluxes illustrate similar response signals (figures not shown). Compared with T255 experiments, T511 experiments show similar response patterns, except a slightly enhanced magnitude in spring and summer, which are consistent with precipitation response patterns (Fig. C.3). Similarly response signals are also found for net surface solar radiation and longwave radiation (figures not shown).

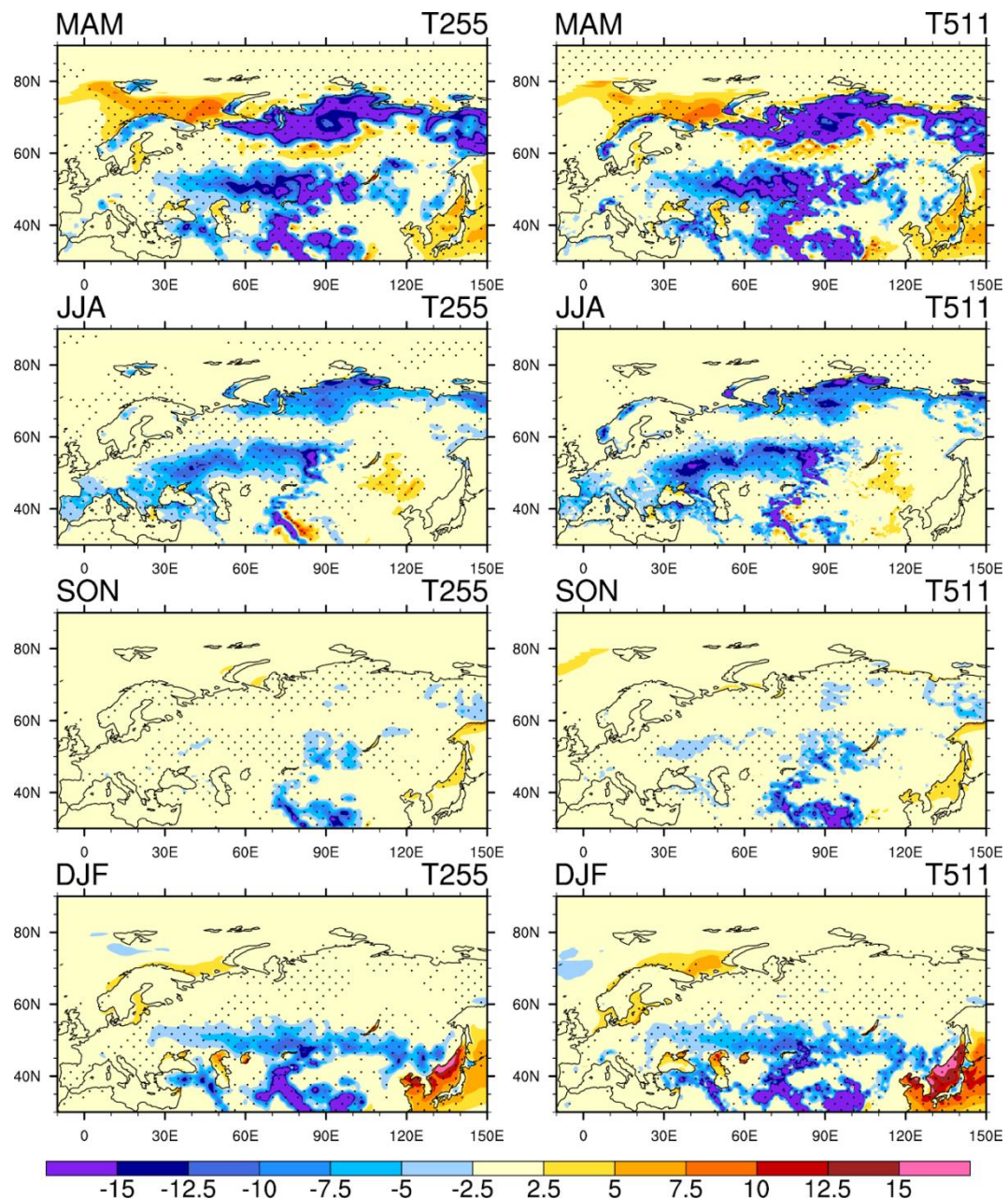


Fig. C.4 Same as Fig. C.2 but for surface net sensible heat fluxes (unit:  $\text{wm}^{-2}$ , positive downward)

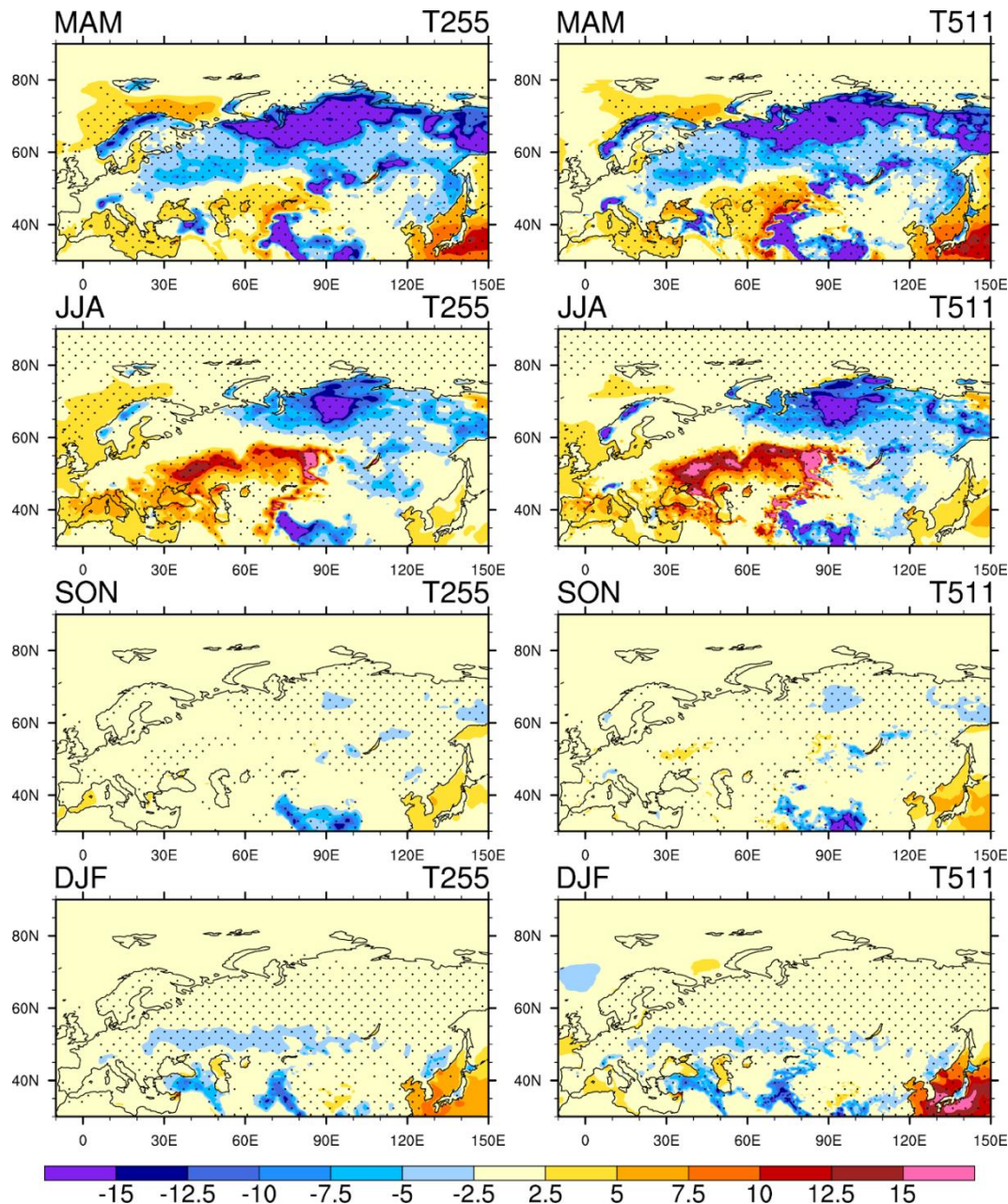


Fig. C.5 Same as Fig. C.2 but for net surface latent heat fluxes (unit:  $\text{wm}^{-2}$ , positive downward)

### C.3.2 Atmospheric circulation response

Above analyses reveal that there are clearly surface responses signals to snow cover reduction over all seasons. Smaller or missing snow cover over land enhances diabatic heating at the surface and in the lower troposphere. This might modifies the stationary wave pattern and transfers less energy from the troposphere to the stratosphere, resulting in a strong polar vortex (Cohen et al. 2007; Furtado et al. 2015). This snow-atmosphere coupling can both regulate the local and remote climate. In this section we will further investigate the influence of snow cover forcing on the atmospheric circulation.

Fig. C.6 shows the seasonal difference of the mean sea level pressure(SLP) between the North Hemisphere experiment and control experiments in T255 and T511 experiments, respectively. In T255 experiments, the reduced snow albedo over the land region warms the

overlying atmosphere and generates negative SLP anomalies. This is particularly obvious in winter and spring. A strong positive SLP anomaly is seen over the ocean, which could partly contribute from sharp land-sea thermal contrast from the anomalous warming over land. In the rest seasons, the SLP anomalies show similar spatial patterns, but the magnitude is much weaker. This implies that the lower atmosphere circulation is largely regulated by the local surface warming. To further examine the mid-tropospheric geopotential height responses, the simulated stationary eddies pattern, which the deviation from the zonal mean 500hPa geopotential fiends are constructed and shown in Fig. C.7. In the North Hemisphere, the strong zonal asymmetry circulation patterns are primarily determined by the complex topography, e.g. the Rockies and Himalayas, and land-sea thermal contrast (Chang, 2009). The variations of stationary wave patterns play an important role in regulating heat and moisture poleward transportation and exhibit different warm/cold conditions over continents. It is apparent that the eddy bias has strong seasonal variations. The spatial stationary wave pattern in winter shows ridges over northwestern North America and western Europe and troughs over northeastern North America and eastern Asia in the control experiment(black contour in Fig. C.7). The ridge and trough are particularly strong over Eurasian. The positive eddy bias pattern over eastern Eurasian indicates that the ridge over western Europe is slightly enhanced, but the trough over East Asia is slightly displaced. The strongest positive bias is located over the Pacific Ocean sector, which is related to large positive surface pressure biases over the Pacific sector in boreal winter (Fig. C.6). The ridge and trough over northern American are slightly southward displaced and the amplitude of the stationary eddy biases is relatively smaller compared to the Pacific sector. The strongest positive geopotential height anomalies occur over high latitude regions in spring. This is consistent with largest warm biases over high latitude regions (Fig. C.2). Compared to T255 experiments, the atmospheric circulation responses have been systematically enhanced in winter and spring in T511 experiments. The impact of horizontal resolution in summer and autumn are minor.

Above analyses show that there are distinct different responses between the western and eastern of Eurasian. The snow cover reduction plays an important role in contributing to polar warm amplification, particularly over Siberia region. Fig. C.8 shows the vertical temperature differences(averaged between 60°E-150°E) between the North Hemisphere experiment and control experiment in T255 and T511 experiments, respectively. In T255 experiments, warm bias in the troposphere and cold biases in the stratosphere implies that systematically reduced snow cover and a weakened Siberia high lead to decreased amount of energy transferring from the troposphere to the stratosphere. The responses are strong in all seasons except in autumn, which implies that upper air is more sensitive to local surface warming, particularly the stratosphere. The cold temperature biases in the stratosphere leads to a strengthening of the polar vortex, as demonstrated in Fig. C.9 by the positive stratospheric zonal-mean zonal-wind anomalies in winter and spring. The stratospheric high-latitude zonal-wind and geopotential height anomalies (figures not shown) are associated with the strengthened polar vortex down into the troposphere and generate opposite-signed zonal-mean zonal-wind anomalies at midlatitudes, which leads to a northward displaced jet. Compared to T255 experiments, T511 experiments tend to lead more robust responses in winter and spring, particularly in winter.

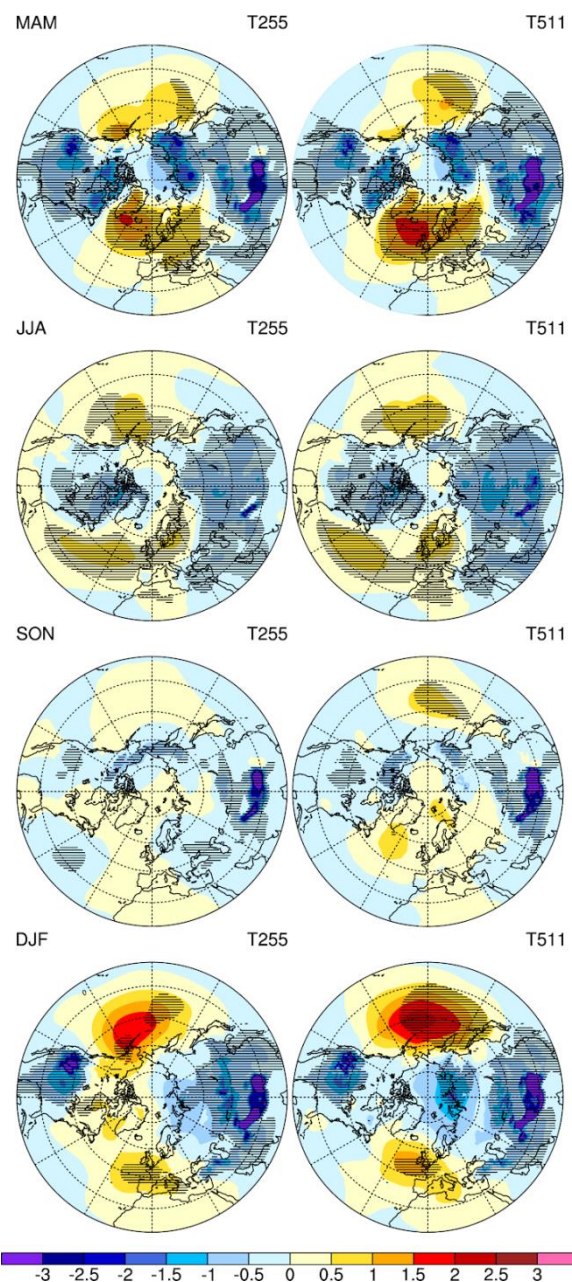


Fig. C.6 Ensemble Mean sea level pressure differences between North Hemisphere experiment and control experiment for MAM, JJA, SON and DJF (Dotted area denotes significant values except 95% confidence level based on a Student's t-test) in T255(Left) and T511 (Right) resolutions (unit:hPa)

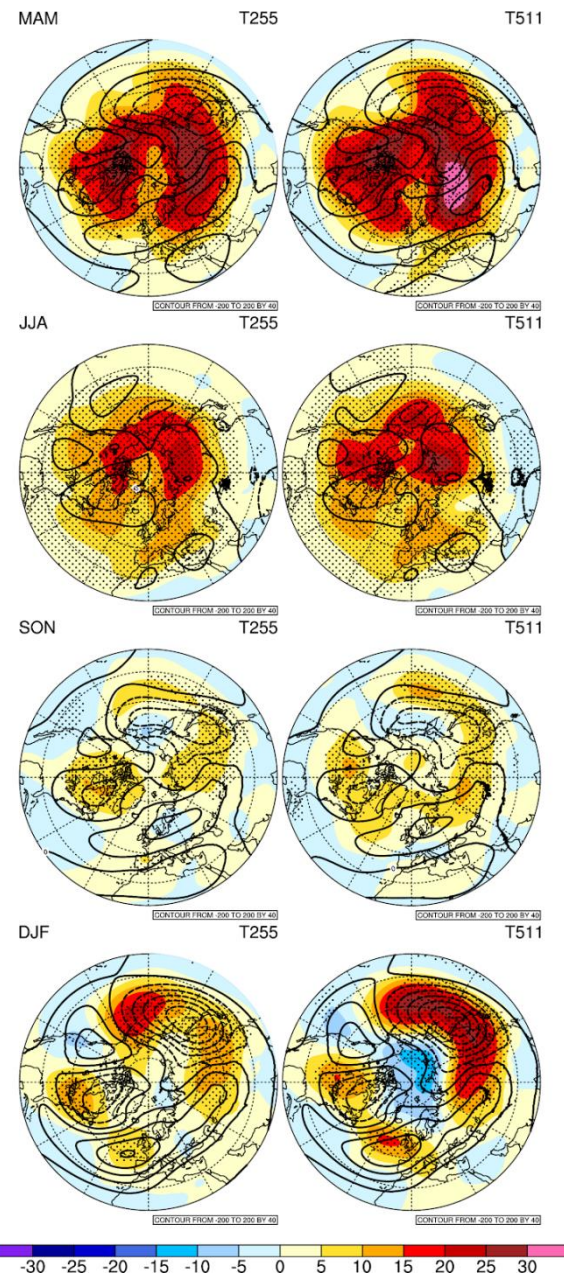


Fig. C.7 Ensemble Mean 500hPa geopotential height differences between North Hemisphere experiment and control experiment for MAM, JJA, SON and DJF( shaded area)( blank lines denote the zonal mean eddy from control experiment) (Dotted area denotes significant values except 95% confidence level based on a Student's t-test) in T255(Left) and T511 (Right) resolutions (unit:meter)

T average between 60E and 150E

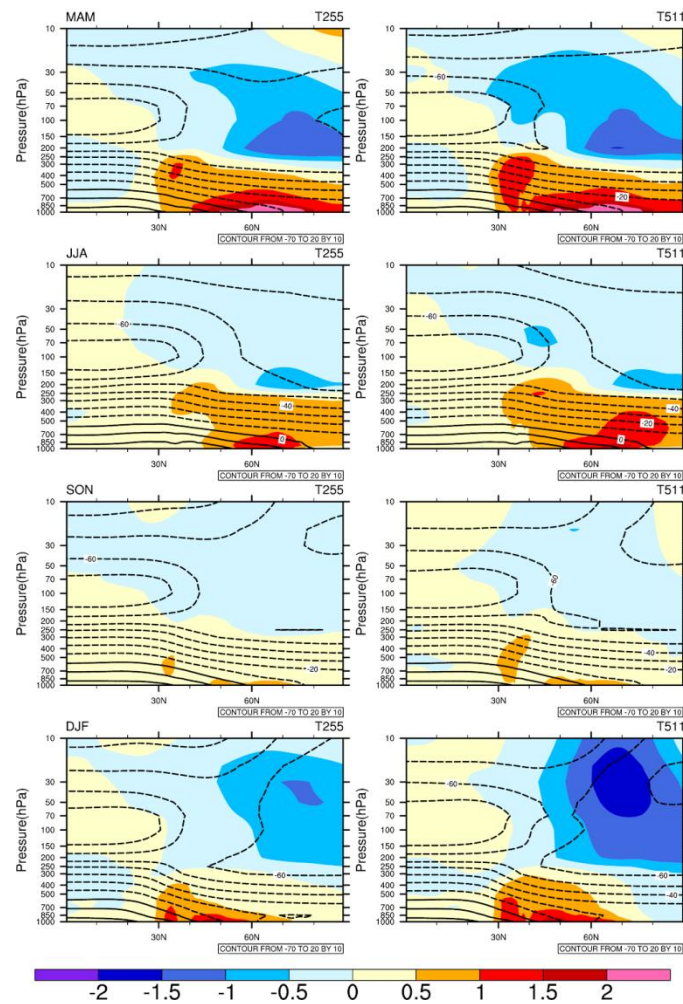


Fig. C.8 Ensemble Mean vertical temperature profile differences (averaged between  $60^{\circ}\text{E}$ - $150^{\circ}\text{E}$ ) between North Hemisphere experiment and control experiment for MAM, JJA, SON and DJF( shaded area)( blank lines denote the zonal mean temperature profile from control experiment) in T255(Left) and T511 (Right) resolutions (unit:K)

U average between 60E and 150E

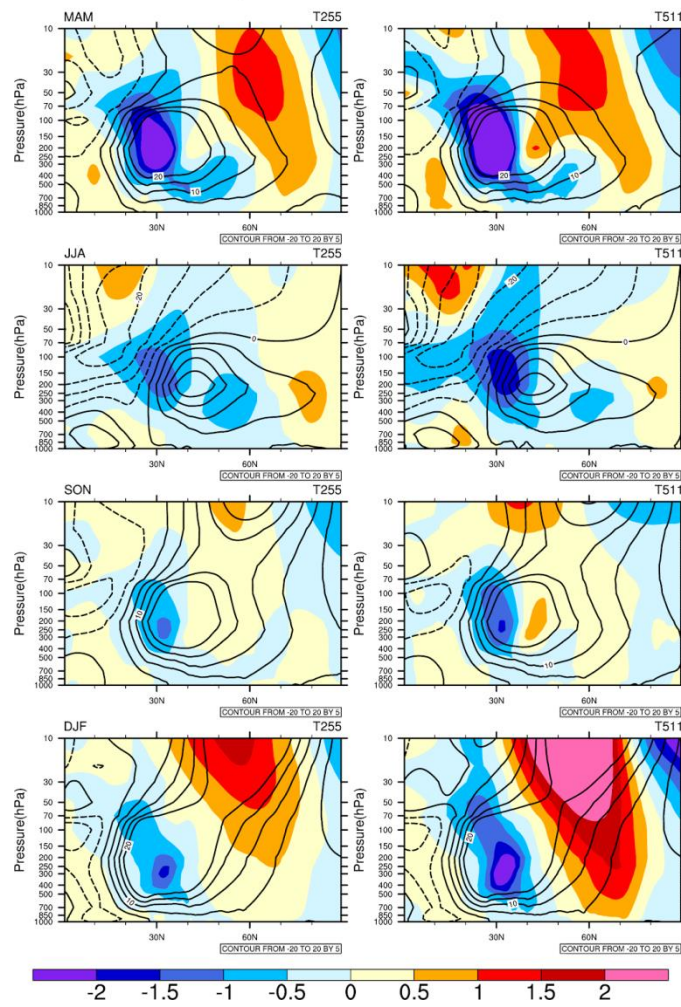


Fig. C.9 Same as Fig. C.8 but for U wind component (unit:m/s)

### C.3.3 The linkage between the atmospheric circulation and European climate

Over Eurasian, NAO determines the degree to which the Arctic air links with the midlatitudes. The phase of NAO has an important impact on interannual variability of Eurasian climate through atmospheric teleconnection. Observational studies imply but do not conclusively prove a causal relationship between snow and the winter NAO and lack of snow over Siberia in autumn favors the positive phase of the NAO. Based on our sensitivity analysis, the most robust responses are in winter and spring. To explore the possible physical mechanisms for this teleconnection and investigate how snow-reduction will impact this snow-NAO relationship. Fig. C.10 illustrated the regression of winter surface temperature onto the standardized winter NAO index in T255 and T511 experiments. In the T255 experiment, the snow-AO teleconnection is well captured in the control experiment. Strong positive correlation in the high latitude regions and negative correlation in the midlatitude. Compared to the control experiment, snow-reduction produces a similarly warm-cold pattern over Eurasian, but the magnitude is slightly weaker, which implies in the T255 experiments the snow cover reduction doesn't favor producing more positive NAO phases. Compared to T255 experiments, although T511 experiments show a weaker correlation, there is a clearly strengthened positive correlation in the T511 sensitivity experiments compared to its control runs. This indicates that the snow cover reduction at high resolution tends to produce more

positive NAO. Fig. C.11 shows the regression of winter precipitation onto the standardized winter NAO index in T255 and T511 experiments. All experiments show the largest impact of snow reduction on precipitation is over the ocean instead of over the land. Compared to the control run, in T255 experiments the negative correlation is reduced in the Atlantic Ocean and enhanced in the Pacific Ocean. While the negative correlation is enhanced in the Atlantic Ocean in the T511 experiment.

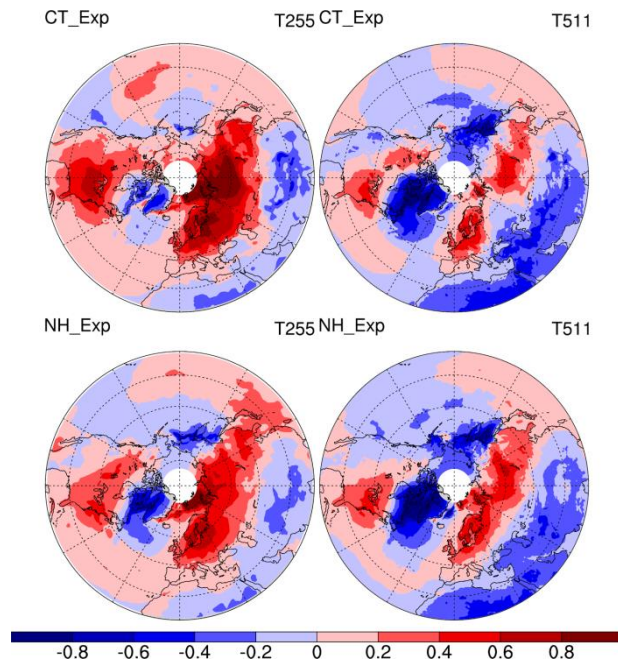


Fig. C.10 Regression of DJF surface temperature onto the NAO index for control experiment(CT\_Exp) and the North Hemisphere experiment(NH\_Exp) in T255 (Left) and T511 (Right) experiments (unit:K)

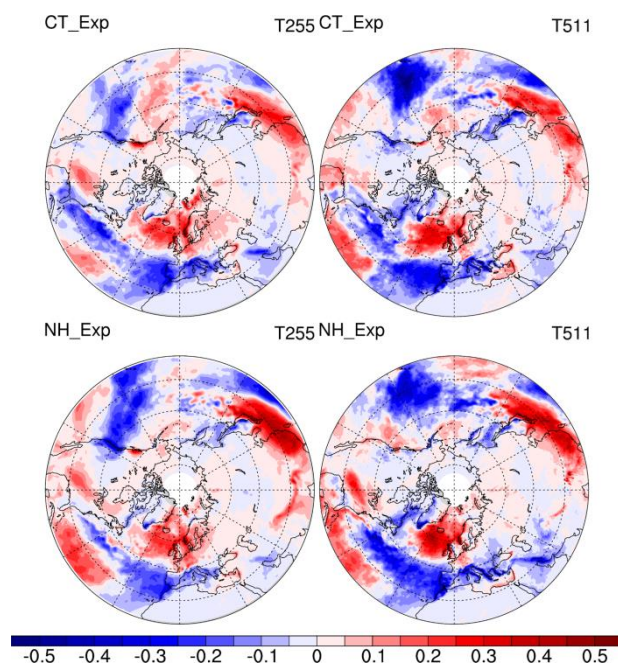


Fig. C.11 Same as Fig. C.10 but for precipitation (unit:mm/day)

## C.4 Results from Eurasian snow albedo reduction experiments

From the above analysis, the snow cover is closely correlated with surface temperature. Lower snow cover is coincident with strong and large-scale surface warming. Similar but weaker temperature signals are observed in the middle and upper troposphere and reversed temperature signals in the stratosphere. Is this warming mainly caused by Eurasian snow cover? Can we still capture a similar response when snow albedo is only reduced over Eurasian region? To further investigate the impact of Eurasina snow cover, a new set sensitivity experiment is performed and analyzed to answer this question.

In general, the Eurasian snow albedo reduction experiments produce very similar patterns over Eurasian region as in the North Hemisphere experiments, except the magnitude of response signals are slightly weaker. Fig. C.12 shows the seasonal mean surface temperature differences between the Eurasian experiments and control experiments for T255 and T511 resolutions, respectively. Over Eurasian region, the warm biases have reduced about 0.25-0.5K compared to the North Hemisphere experiment (Fig. C.2). However, there are no obvious warm biases out of Eurasian region (figures not shown). This implies that the largest local warming is mainly contributed by local snow cover reduction. Similarly response signals changes are also found in other surface parameters,e.g. Precipitation, heat fluxes (figures not shown). However, this slightly weakened warm biases have much strong impact on the circulation variations, particularly at the uppair. Seen from Fig. C.13, the mean sea level pressure is only slightly altered in all seasons at both T255 and T511 resolutions. The vertical temperature profile differences are strongly reduced (Fig. C.14) . Compared to the North Hemisphere experiment, a cooler surface leads to more energy absorption in the stratosphere. A slightly weakened polar vortex associated with a weakened westly jet is also found in the Eurasian experiment (figures not shown).

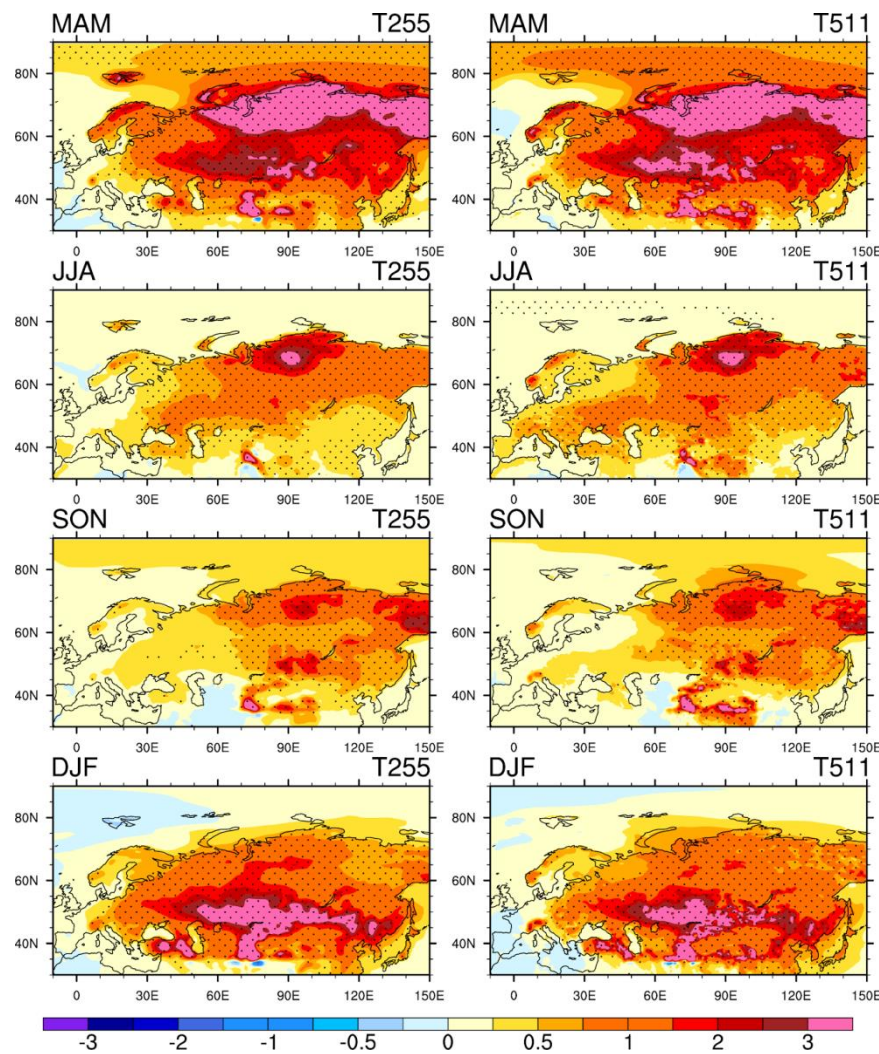


Fig. C.12 Ensemble Mean surface air temperature differences between the Eurasian experiment and control experiment for MAM, JJA, SON and DJF (Dotted area denotes significant values except 95% confidence level based on a Student's t-test) in T255(Left) and T511 (Right) resolutions

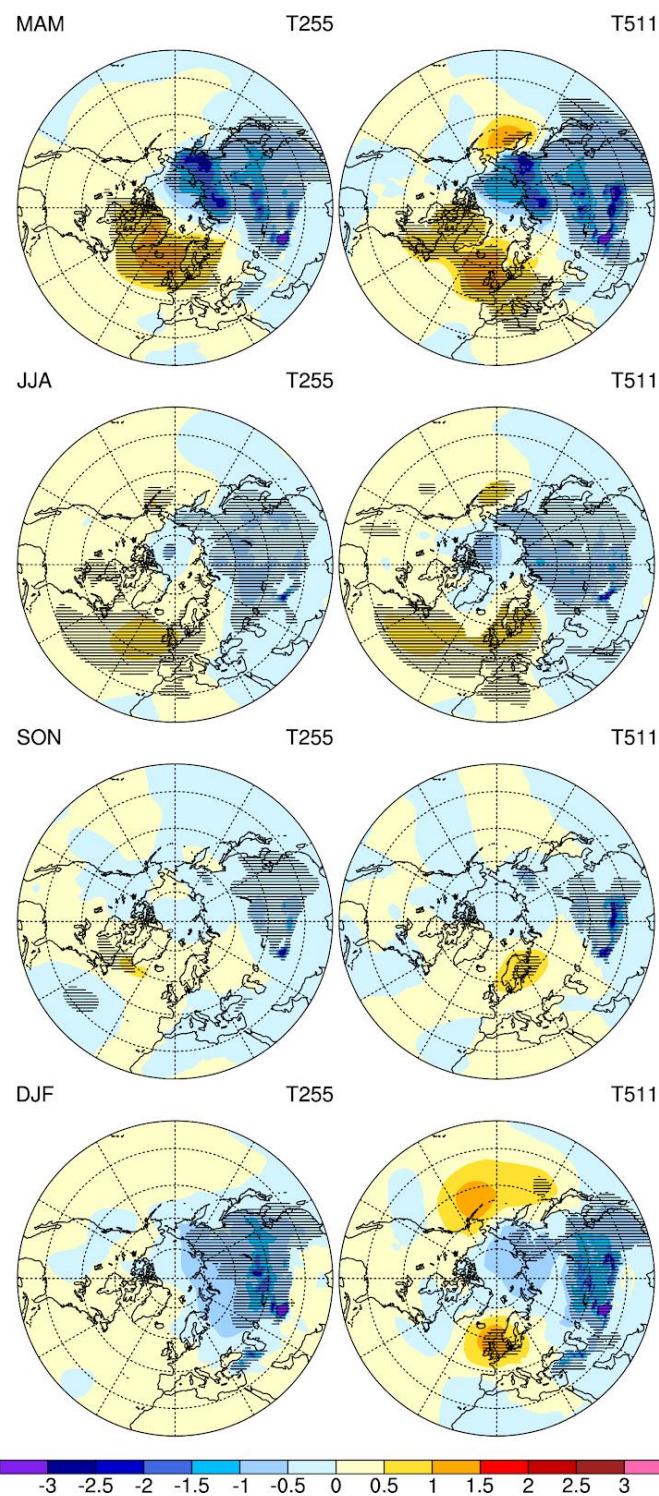


Fig. C.13 Ensemble Mean sea level pressure differences between the Eurasian experiment and control experiment for MAM, JJA, SON and DJF (Dotted area denotes significant values except 95% confidence level based on a Student's t-test) in T255(Left) and T511 (Right) resolutions (unit:hPa)

### T average between 60E and 150E

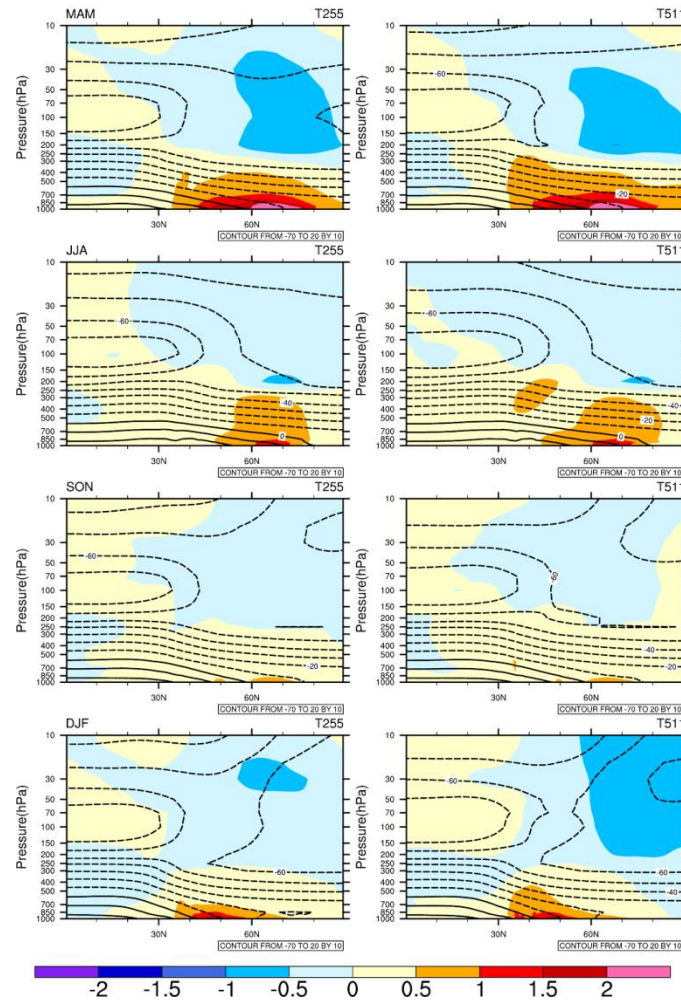


Fig. C.14 Ensemble Mean vertical temperature profile differences (averaged between 60°E-150°E) between the Eurasian experiment and control experiment for MAM, JJA, SON and DJF (shaded area)( blank lines denote the zonal mean temperature profile from control experiment) in T255(Left) and T511 (Right) resolutions (unit:K)

## C.5 Short summary

In this study, the impact of the North Hemisphere and Eurasian snow cover reduction on European climate are investigated. Both experiments indicate the reduced snow cover is closely correlated with surface temperature. Lower snow cover is coincident with strong and large-scale surface warming. Similar but weaker temperature signals are observed in the middle and upper troposphere and reversed temperature signals in the stratosphere. Reduced snow cover is also characterized by surface heat gain, which is accompanied by enhanced turbulent and radiative fluxes. The mean sea level pressure pattern is weakened over land in all snow cover reduction experiments. This leads to a decreased amount of energy transferring from the troposphere to the stratosphere and strong polar vortex. High resolution experiments show similar response patterns, but with slightly enhanced magnitude, mainly in winter and spring. The major response differences between the North Hemisphere and Eurasian experiments are the magnitude of response signal over Eurasian. The response signals are slightly weaker in Eurasian snow reduction experiments, and impact of snow cover reduction in Eurasian experiment is mainly confined into Eurasian region and only have a very minor impact on the rest regions. This implies that Eurasian

climate is also largely influenced by the snow reduction in the North American through teleconnection.

## References

- Allen, R. J., and C. S. Zender, 2011: Forcing of the Arctic Oscillation by Eurasian snow cover. *J. Climate*, 24, 6528–6539
- Armstrong, R. L. & Brodzik, M. J. 2001. Recent Northern Hemisphere snow extent: a comparison of data derived from visible and microwave satellite sensors. *Geophysical Research Letters*, 28, 3673–3676.
- Alfieri L, Bisselink B, Dottori F, Naumann G, de Roo A, Salamon P, Wyser K and Feyen L 2017 Global projections of river flood risk in a warmer world, *Earth's Future*, doi:10.1002/2016EF000485
- Baker, D. G., D. L. Ruschy, R. H. Skaggs, and D. B. Wall (1992), Air temperature and radiation depressions associated with snow cover, *J. Appl. Meteorol.*, 31, 247–254
- Brown R. D. and Robinson D. A., 2011: Northern Hemisphere spring snow cover variability and change over 1922–2010 including an assessment of uncertainty *Cryosphere*, 5, 219–29
- Chang, E., 2009: Diabatic and orographic forcing of northern winter stationary waves and storm tracks. *J. Climate*, 22, 670–688.
- Chen, X. , Liang, S. , Cao, Y. , He, T. , and Wang, D. , 2015: Observed contrast changes in snow cover phenology in northern middle and high latitudes from 2001–2014. *Scientific Reports* , 5: doi <http://dx.doi.org/10.1038/srep16820>.
- Cohen, J. and D. Entekhabi, 1999: Eurasian snow cover variability and Northern Hemisphere climate predictability, *Geophys. Res. Lett.*, 26, 345-348
- Cohen J, Barlow M, Kushner PJ, Saito K (2007) Stratosphere–troposphere coupling and links with Eurasian land surface variability. *J Clim* 20:5335–5343
- Cohen, J., J. Jones, J. C. Furtado, and E. Tziperman (2013), Warm Arctic, cold continents: A common pattern related to Arctic sea ice melt, snow advance, and extreme winter weather, *Polar Oceanogr.* , 26, 152–160.
- Derkson, C., and E. LeDrew, 2000. Variability and change in terrestrial snow cover: Data ququisition and links to the atmosphere, *Prog. Phys. Geogr.*, 24, 469-498
- Fletcher, C. G., S. C. Hardiman, P. J. Kushner, and J. Cohen, 2009: The dynamical response to snow cover perturbations in a large ensemble of atmospheric GCM integrations. *J. Climate*, 22, 1208–1222.
- Fallot, J. M., R. G. Barry, and D. Hoogstrate (1997), Variations of mean cold season temperature, precipitation and snow depths during the last 100 years in the former Soviet Union (FSU), *Hydrol. Sci.* , 42, 301–327.
- Furtado, J. C., Cohen, J. L., Butler, A. H., Riddle, E. E., & Kumar, A. (2015). Eurasian snow cover variability and links to winter climate in the CMIP5 models. *Climate Dynamics*, 45(9-10), 2591–2605. <https://doi.org/10.1007/s00382-015-2494-4>

Gong, G., Entekhabi, D., Cohen, J., & Robinson, D. (2004). Sensitivity of atmospheric response to modeled snow anomaly characteristics. *Journal of Geophysical Research*, 109, D06107. <https://doi.org/10.1029/2003JD004160>

Hardiman, S. C., Kushner, P. J., & Cohen, J. (2008). Investigating the ability of general circulation models to capture the effects of Eurasian snow cover on winter climate. *Journal of Geophysical Research*, 113, D21123. <https://doi.org/10.1029/2008JD010623>

Haarsma, R. J., Roberts, M. J., Vidale, P. L., Senior, C. A., Bellucci, A., Bao, Q., Chang, P., Corti, S., Fučkar, N. S., Guemas, V., von Hardenberg, J., Hazeleger, W., Kodama, C., Koenigk, T., Leung, L. R., Lu, J., Luo, J.-J., Mao, J., Mizielinski, M. S., Mizuta, R., Nobre, P., Satoh, M., Scoccimarro, E., Semmler, T., Small, J., and von Storch, J.-S.: High Resolution Model Intercomparison Project (HighResMIP v1.0) for CMIP6, *Geosci. Model Dev.*, 9, 4185–4208, <https://doi.org/10.5194/gmd-9-4185-2016>, 2016.

Hazeleger, W., et al. (2012), EC-Earth V2.2: Description and validation of a new seamless earth system prediction model, *Clim. Dyn.*, 39 (11), 2611–2629, doi:10.1007/s00382-011-1228-5.

Hazeleger, W., V. Guemas, B. Wouters, S. Corti, I. Andreu-Burillo, F. J. Doblas-Reyes, K. Wyser, and M. Caian (2013), Multiyear climate predictions using two initialization strategies, *Geophys. Res. Lett.*, 40(9), 1794–1798, doi:10.1002/grl.50355

Matsumura, S., & Yamazaki, K. (2012). Eurasian subarctic summer climate in response to anomalous snow cover. *Journal of Climate*, 25(4), 1305–1317. <https://doi.org/10.1175/2011JCLI4116.1>

Jones, H. G., Pomeroy, J. W., Walker, D. A. & Hoham, R. W. 2001. *Snow Ecology – An Interdisciplinary Examination of Snow-Covered Ecosystems*. Cambridge University Press, 378 pp

Peings, Y., and H. Douville, 2010: Influence of the Eurasian snow cover on the Indian summer monsoon variability in observed climatologies and CMIP3 simulations. *Climate Dyn.*, 34, 643–660, doi:10.1007/s00382-009-0565-0.

Peings, Y., R. Alkama, and B. Decharme, 2011: Snow contribution to springtime atmospheric predictability over the second half of the twentieth century. *Climate Dyn.*, 37, 985–1004, doi:10.1007/s00382-010-0884-1

Peings Y., D. Saint-Martin, H. Douville (2012) A Numerical Sensitivity Study of the Influence of Siberian Snow on the Northern Annular Mode. *Journal of Climate*, 25, 592–607.

Peng, S., Shilong Piao, Philippe Ciais, Pierre Friedlingstein, Liming Zhou, and Tao Wang, 2013, Change in snow phenology and its potential feedback to temperature in the Northern Hemisphere over the last three decades. *Environ. Res. Lett.* 8, 014008

Robinson, D.A.; Dewey, K.F.; Heim, R.R. Global Snow Cover Monitoring: An Update. *Bull. Am. Meteorol. Soc.* 1993, 74, 1689–1696.

Robinson. D.A., and A. Frei. 2000. [Seasonal variability of Northern Hemisphere snow extent using visible satellite data.](#) *Professional Geographer* 52(2): 307-315.

Tyrrell, N. L., Karpechko, A. Y., Räisänen, P. (2018). The influence of Eurasian snow extent on the northern extratropical stratosphere in a QBO resolving model. *Journal of Geophysical Research: Atmospheres*, 123, 315–328. <https://doi.org/10.1002/2017JD027378>



## Report from ECMWF

The response of the atmosphere to low snow conditions are analysed using twin atmosphere-only ensemble simulations with the low (WP5-AMIP-Snow LR) and high-resolution (WP5-AMIP-Snow HR) versions of the ECMWF-IFS climate model configuration (Roberts et al, 2018). Two sets of idealized experiments were performed with the prescribed snow albedo set to 0.3 everywhere except glaciers including Antarctica (Table C.1). The runs were initialized on 01-01-1980 from the respective LR and HR Stream 1 highresSST-present. The control simulation for these experiments are taken from the Stream 2 highresSST-present simulations. Six ensembles from these experiments for the period 1981-2010 constitute the CONTROL LR and CONTROL HR to complement six ensembles from the WP5-AMIP-Snow LR and HR simulations.

The impact of setting snow albedo to 0.3 as expectedly results in a reduction in snow depth with the largest signal in March to May (MAM, Figure C.15a, C.15.b) following the maxima in seasonal snow in February-March (not shown), and is stronger than the response in the peak cold season, December to January (DJF, Figure C.15c, C.15d). There are no prominent differences between the LR and HR patterns in both seasons.

The near surface atmospheric response to the reduced snow is shown in Figure C.16. There is a large surface warming signal across the Northern Hemisphere during MAM (Figure C.16a, C.15b) as a result of the reduced snowpack. Compared to MAM, the signal in DJF (Figure C.16c, C.15d) is weaker especially in the higher latitudes. The warming signal is weak in June to August (JJA, Figure C16e, C.15f) and in September to October (SON, Figure C16g, C.15h) when the largest differences are confined to the Tibetan Plateau. Again, the impact of high resolution is not very evident in the near surface response with warming patterns being largely similar across LR and HR. It is to be noted that mean surface climate in ECMWF-IFS climate configuration is largely insensitive to increased atmospheric resolution in the Stream 1 highresSST-present atmosphere-only simulations (Roberts et al., 2018).

In response to the surface warming, there is a local reduction in mean sea level pressure (MSLP) over the continent that sets up a strong circulation response in the mid-latitudes (30N-60N) with warm MSLP over the mid-latitude oceans in MAM (Figure C.17a, C.16b) and DJF (Figure C.17g, C.16h). Unlike the near surface temperature response however, the signals in MSLP are different in LR and HR especially in the north Atlantic sector and Arctic in DJF where there is positive MSLP response in LR over the Arctic and Greenland whereas in HR the response if of the opposite sign over the Arctic.

The upper air circulation patterns also show a robust response to snow reduction (Figure C.18) with an enhanced mid-latitude jet in MAM. The summer time circulation in HR (Figure C.18c,d) over Europe is stronger than in LR. Further, unlike at the surface, the upper air response to maxima in snow reduction in MAM appear to extend into the Autumn (SON) over Eurasia and extratropical north Pacific.

Finally, the impact on some aspects of the impact on interannual variability is assessed. An EOF analysis of interannual mean sea level pressure over the extratropical north Atlantic is performed. The leading mode (Figure C.19) shows the North Atlantic Oscillation (NAO) pattern. The NAO response in LR is consistent with a reduction in snow over Eurasia with an enhanced and more robust high-pressure centre of action in WP5-AMIP-Snow LR compared to CONTROL LR. In comparison, the differences in HR is less prominent with a robust NAO pattern in both WP5-AMIP-Snow and CONTROL. However, the low-pressure centre of action seems to be more pronounced in WP5-AMIP-Snow HR compared to CONTROL LR.

In summary, there is a strong surface and upper air response in model mean state to reduced snow with the largest impacts in MAM. However, the impact of HR over LR is less dramatic which is perhaps largely due to the climate attractor of the ECMWF-IFS model being less sensitive to the delta in resolution increase.

#### *References:*

Roberts, C. D., Senan, R., Molteni, F., Boussetta, S., Mayer, M., and Keeley, S. P. E.: Climate model configurations of the ECMWF Integrated Forecasting System (ECMWF-IFS cycle 43r1) for HighResMIP, *Geosci. Model Dev.*, 11, 3681–3712, <https://doi.org/10.5194/gmd-11-3681-2018>, 2018.

Experiment Name	Description
WP5-AMIP-Snow LR	<ul style="list-style-type: none"> <li>• Tco199 (~50km) cubic octahedral grid</li> <li>• Ensemble members: 6</li> <li>• Snow-albedo: 0.3 everywhere except glaciers</li> <li>• 1980-2014</li> <li>• Initialised from stream 1 ECMWF-IFS-LR highresSST-present on 01-01-1980</li> </ul>
WP5-AMIP-Snow HR	<ul style="list-style-type: none"> <li>• Tco399 (~25 km) cubic octahedral grid</li> <li>• Ensemble members: 6</li> <li>• Snow-albedo: 0.3 everywhere except glaciers</li> <li>• 1980-2014</li> <li>• Initialised from stream 1 ECMWF-IFS-HR highresSST-present on 01-01-1980</li> </ul>
CONTROL LR	<ul style="list-style-type: none"> <li>• Tco199 (~50km)</li> <li>• Ensemble members: 6</li> <li>• Subset of ECMWF-IFS-LR Stream 2 highresSST-present simulation</li> </ul>
CONTROL HR	<ul style="list-style-type: none"> <li>• Tco399 (~25 km)</li> <li>• Ensemble members: 6</li> <li>• Subset of ECMWF-IFS-HR Stream 2 highresSST-present simulation</li> </ul>

Table 1: Summary of model configurations

**Snow Depth (cm) 1981-2010: WP5-AMIP-Snow minus CONTROL**

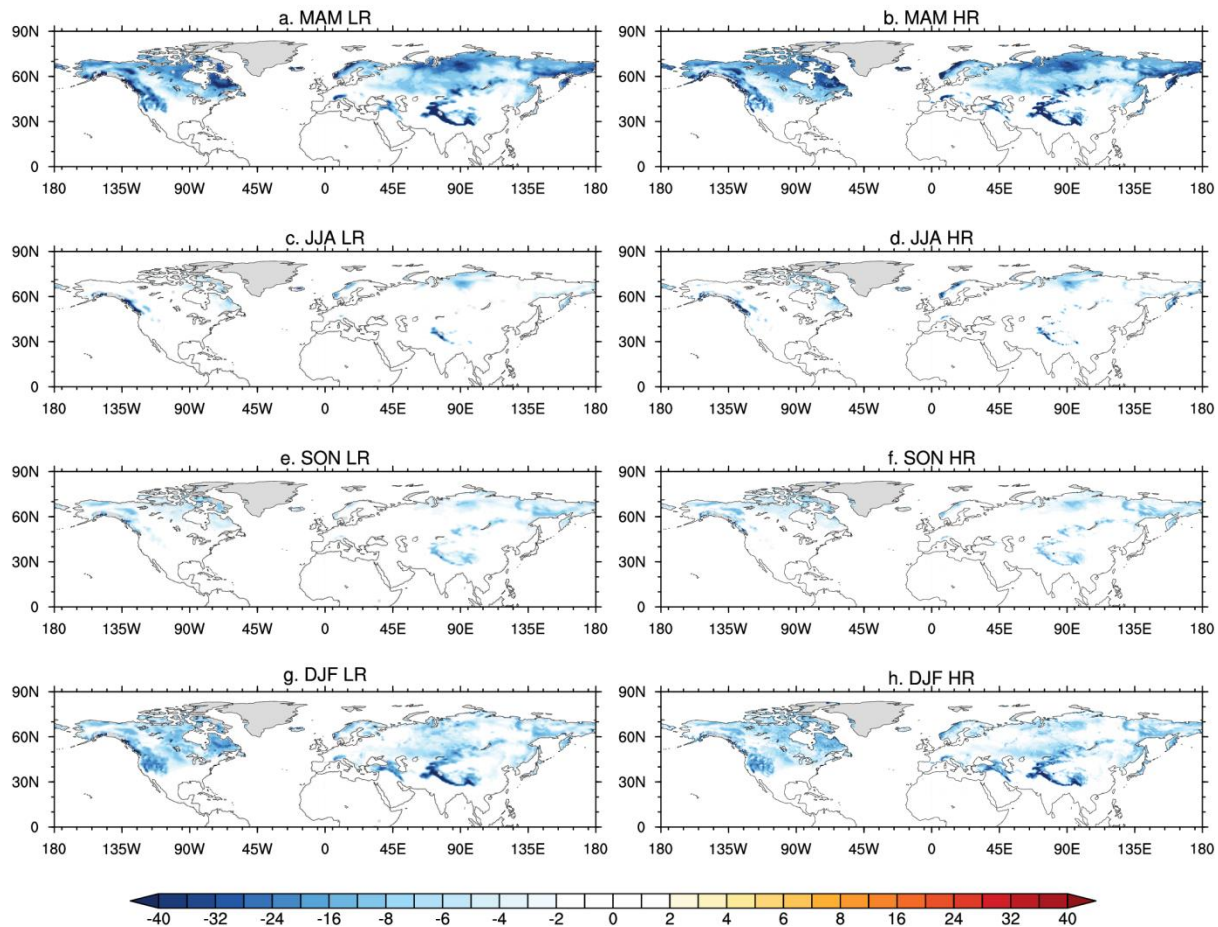


Figure C.15: Ensemble mean difference in northern hemispheric snow depth (cm) between WP5-AMIP-Snow and CONTROL experiments averaged over 1981-2010 for March to May (a, b; MAM), June to August (c, d; JJA), September to November (e, f; SON) and December to February (g, h; DJF) for low resolution (LR; left panels) and high resolution (HR; right panels).

**2m Temperature ( $^{\circ}\text{C}$ ) 1981-2010: WP5-AMIP-Snow minus CONTROL**

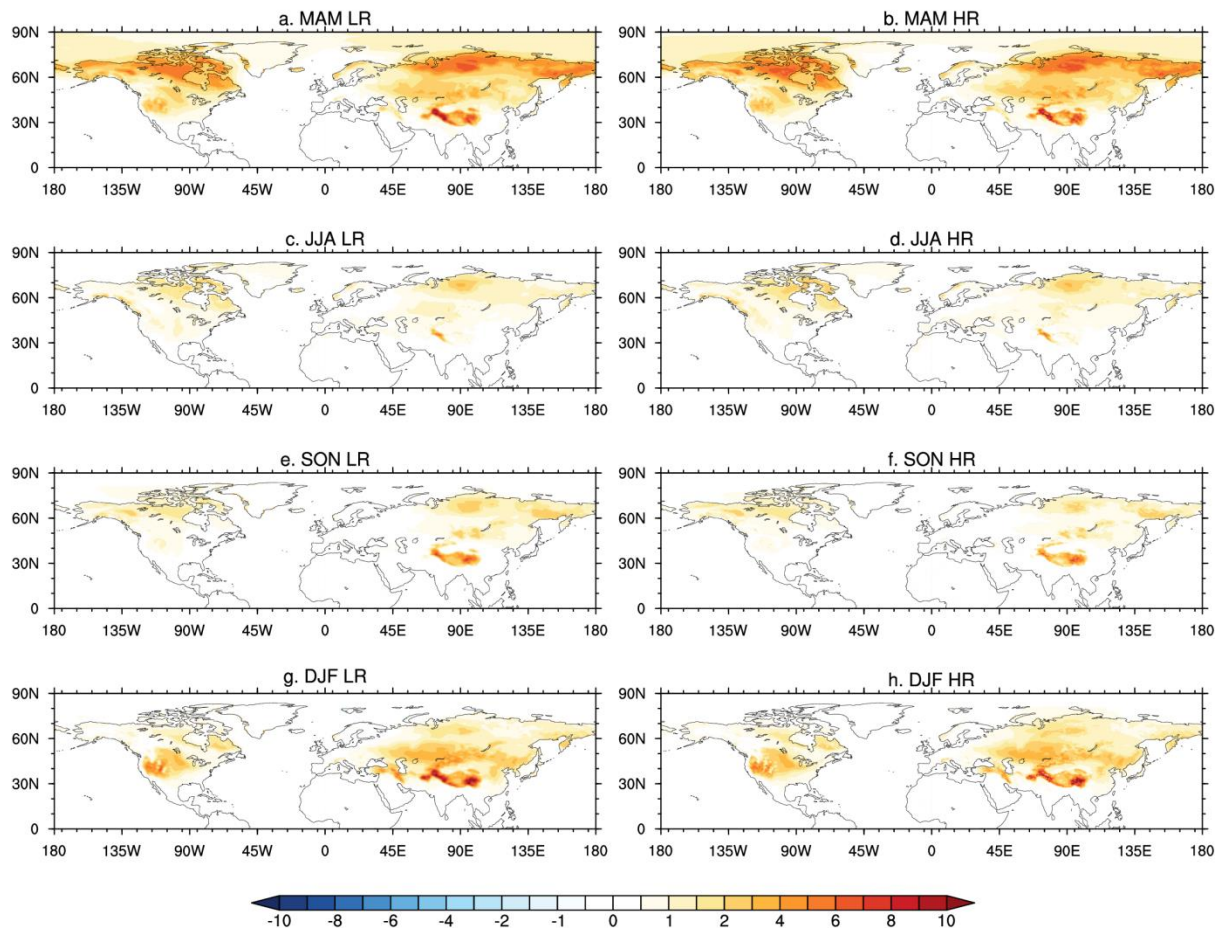


Figure C.16: Same as Fig. C.15, but for 2m temperature (C).

**Sea Level Pressure (hPa) 1981-2010: WP5-AMIP-Snow minus CONTROL**

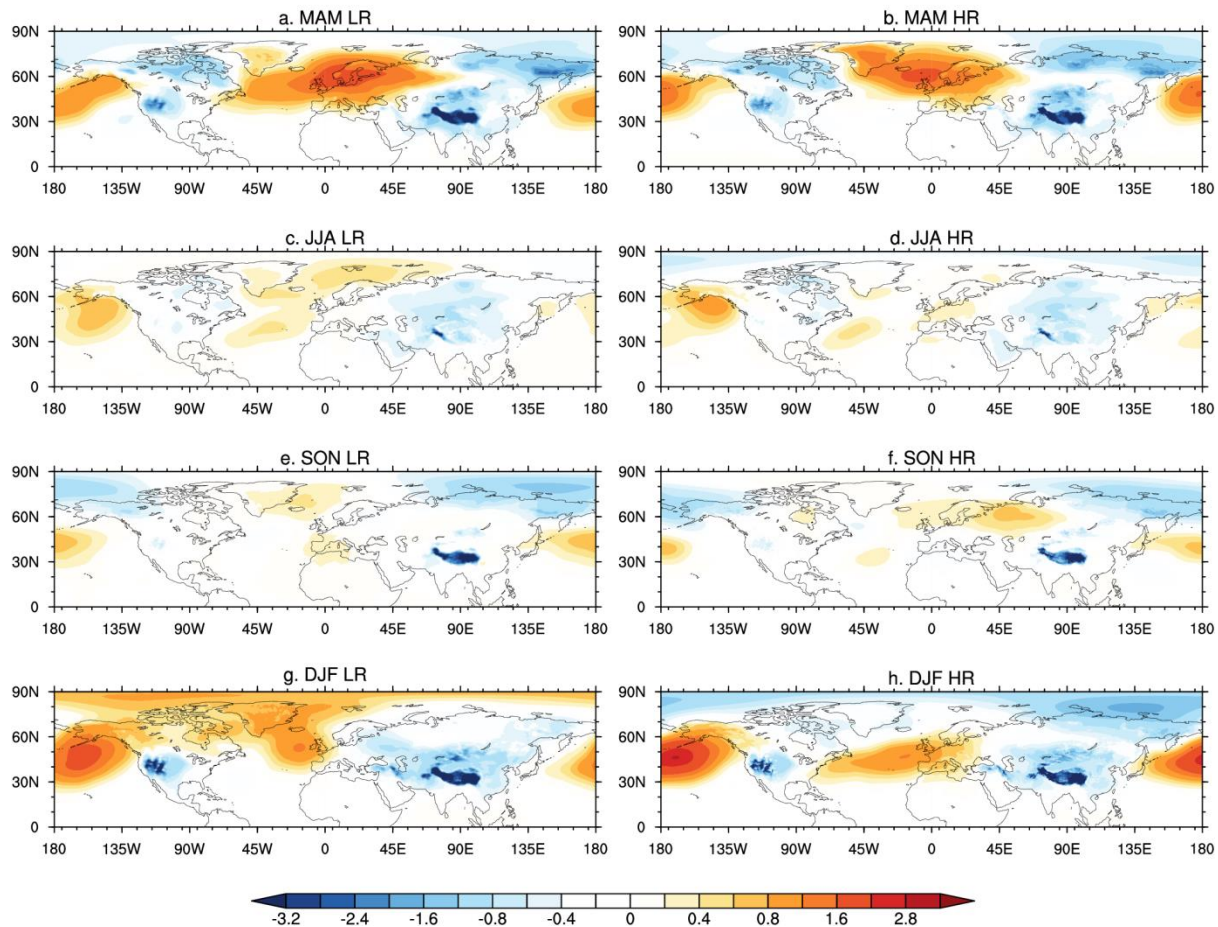


Figure C.17: Same as Fig. C.15, but for mean sea level pressure (hPa).

**500 hPa Geopotential Height (m) 1981-2010: WP5-AMIP-Snow minus CONTROL**

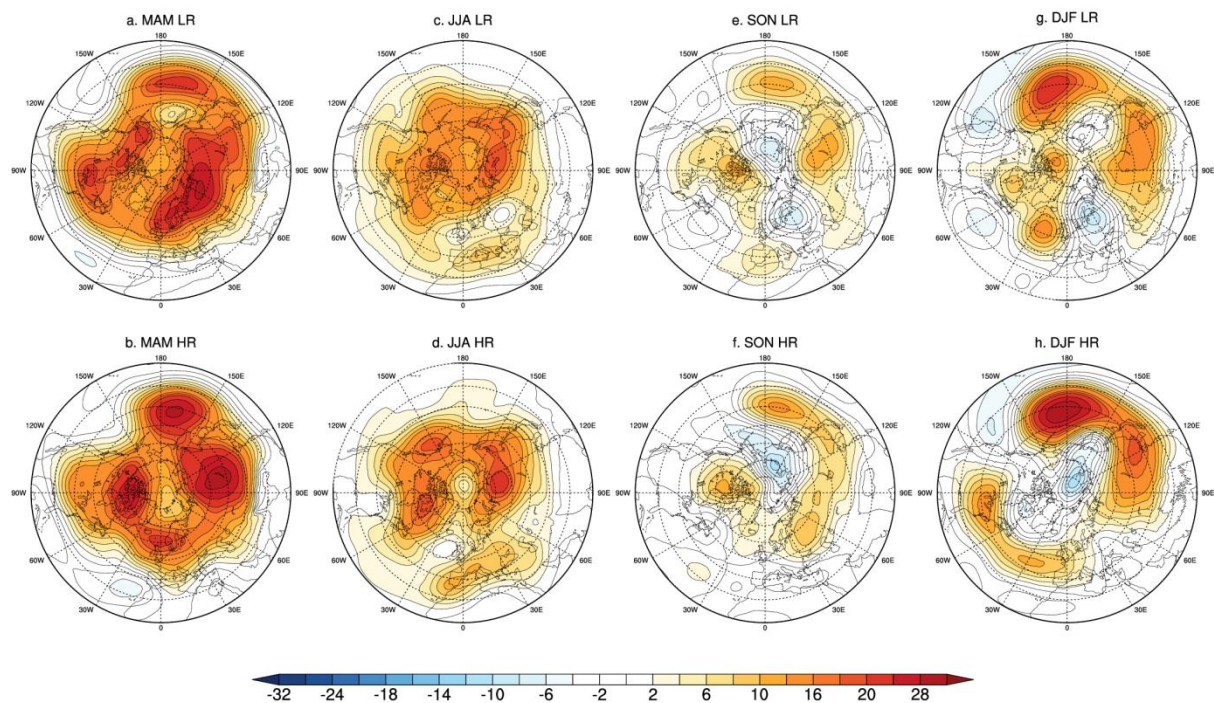


Figure C.18: Same as Fig. C.17 but for 500 hPa Geopotential height (m) in LR (top panels) and HR (bottom panels).

**NAO: EOF1 of Mean Sea Level Pressure (hPa) DJF 1981-2010**

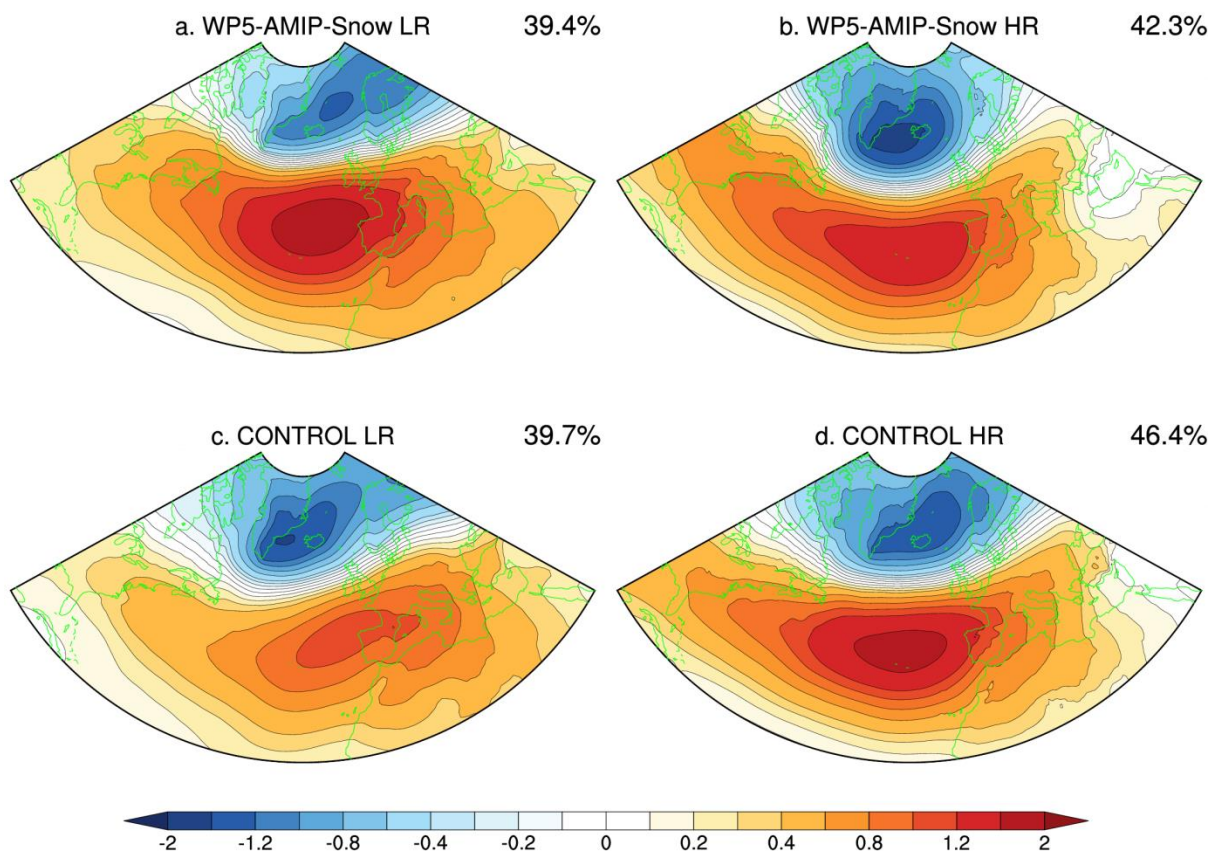


Figure C.19: Leading mode of interannual variability in mean sea level pressure over the extratropical north Atlantic: the NAO in (a,c) low and (b,d) high resolutions of (a,b) WP5-AMIP-Snow and (c,d) CONTROL experiments.